

The Angular Three-Point Correlation Function in the Quasilinear Regime

Ari Buchalter^{*1}, Marc Kamionkowski^{†2}, and Andrew H. Jaffe ^{‡3}

^{*}Department of Astronomy and Columbia Astrophysics Laboratory, Columbia University,
550 West 120th St., New York, NY 10027

[†]Department of Physics and Columbia Astrophysics Laboratory, Columbia University, 550
West 120th St., New York, NY 10027

[‡]Center for Particle Astrophysics, 301 LeConte Hall, University of California, Berkeley,
CA 94720

ABSTRACT

We calculate the normalized angular three-point correlation function (3PCF), q , as well as the normalized angular skewness, s_3 , assuming the small-angle approximation, for a biased mass distribution in flat and open cold-dark-matter (CDM) models with Gaussian initial conditions. The leading-order perturbative results incorporate the explicit dependence on the cosmological parameters, the shape of the CDM transfer function, the linear evolution of the power spectrum, the form of redshift distribution function, and linear and nonlinear biasing, which may be evolving. Results are presented for different redshift distributions, including that appropriate for the APM Galaxy Survey, as well as for a survey with a mean redshift of $\bar{z} \simeq 1$ (such as the VLA FIRST Survey). Qualitatively, many of the results found for s_3 and q are similar to those obtained in a related treatment of the spatial skewness and 3PCF (Buchalter & Kamionkowski 1999), such as a leading-order correction to the standard result for s_3 in the case of nonlinear bias (as defined for unsmoothed density fields), and the sensitivity of the configuration dependence of q to both cosmological and biasing models. We show that since angular CFs are sensitive to clustering over a range of redshifts, the various evolutionary dependences included in our predictions imply

¹ari@astro.columbia.edu

²kamion@phys.columbia.edu

³jaffe@cfpa.berkeley.edu

that measurements of q in a deep survey might better discriminate between models with different histories, such as evolving vs. non-evolving bias, that can have similar spatial CFs at low redshift. Our calculations employ a derived equation—valid for open, closed, and flat models—for obtaining the angular bispectrum from the spatial bispectrum in the small-angle approximation.

Subject headings: large scale structure of the universe — cosmology: theory — galaxies: clustering — galaxies: statistics

1. INTRODUCTION

Characterization of the initial distribution of density perturbations and understanding their subsequent evolution into present-day structures are among the central aims of cosmology. Particular attention has been focused on the low-redshift distribution of matter over large scales, which can probe the linear physics of the early universe and therefore test models for the origin of large-scale structure, such as inflation. The n -point correlation functions⁴ (CFs) have become the most widely used statistical tools to quantify the observed distribution of matter, in part because they can be easily related to the predictions of such models and thus discriminate between them. In principle, recovering the current distribution of density perturbations is straightforward; one simply maps the three-dimensional distribution of mass with a sufficiently large redshift survey. Existing redshift surveys, however, typically contain relatively small numbers of objects, have inconvenient shapes, and necessarily suffer from redshift-space distortions, all of which make it difficult to obtain precise CF measurements, particularly for the higher-order functions.

Another possibility is to map the angular distribution of galaxies as projected onto the surface of the sky. Angular surveys can sample larger volumes of space and contain greater numbers of objects. Furthermore, the effects of redshift distortions need not be considered in an angular survey. Thus, if the redshift distribution is well constrained, as is often the case for large angular surveys, angular CFs can in practice provide far greater statistical power and more insight into the evolution of clustering, than sparser, redshift-survey data (Groth & Peebles 1977; Fry & Seldner 1982; Jing, Mo, & Börner 1991; Baugh & Efstathiou

⁴The term “correlation function” is understood throughout to refer to the connected, or reduced, correlation function. Note that the n -point CFs are valid statistics only if the universe is homogeneous on large scales. We invoke the assumptions of large-scale homogeneity and isotropy, so that the CFs depend only relative distances and are independent of orientation.

1993; Cappi & Maurogordato 1995; Cress *et al.* 1996; Maddox, Efstathiou & Sutherland 1996; Gaztañaga & Baugh 1998; Cress & Kamionkowski 1998).

To date, angular-clustering studies have focussed primarily on the angular two-point correlation function (2PCF), $\varpi(\theta)$, but with advent of new, deep surveys at various wavelengths (radio, optical, IR, x-ray) and more powerful computing resources, increasing attention is being focused on higher-order CFs. These are particularly important in assessing primordial Gaussianity (Fry 1984; Goroff *et al.* 1986; Bernardeau 1994; Fry & Scherrer 1994; Gaztañaga & Bernardeau 1998; White 1998; Scoccimarro *et al.* 1998; Scoccimarro, Couchman, & Frieman 1998), since to leading order they, unlike the 2PCF, reflect the inherently nonlinear gravitational amplification of the initial fluctuations. Furthermore, they contain information about the cosmological parameters (Bouchet *et al.* 1992; Juszkiewicz, Bouchet, & Colombi 1993; Gaztañaga, Croft, & Dalton 1995; Bouchet *et al.* 1995; Catelan *et al.* 1995; Martel 1995; Jing & Börner 1997; Szapudi *et al.* 1998; Kamionkowski & Buchalter 1998) and about the nonlinear bias between the observed and underlying density distributions (Jensen & Szalay 1986; Szalay 1988; Fry & Gaztañaga 1993; Frieman & Gaztañaga 1994; Fry 1994; Jing 1997; Matarrese, Verde, & Heavens 1997), which cannot be obtained from $\varpi(\theta)$.

In particular, the angular three-point correlation function (3PCF), $Z(\theta_{12}, \theta_{23}, \theta_{31})$, and relatedly, the normalized angular skewness, $s_3(\Theta)$ (proportional to Z evaluated at zero lag, for a distribution smoothed over angular scale Θ), are the lowest-order intrinsically nonlinear statistics and can therefore yield important constraints on models of structure formation. Moreover, if different populations are differently biased relative to the underlying mass distribution then measuring the angular 3PCFs of these populations can provide multiple, complementary constraints. Measurements of s_3 , as well as the normalized angular 3PCF, $q(\theta_{12}, \theta_{23}, \theta_{31}) = Z(\theta_{12}, \theta_{23}, \theta_{31}) / [\varpi(\theta_{12})\varpi(\theta_{23}) + \varpi(\theta_{12})\varpi(\theta_{31}) + \varpi(\theta_{23})\varpi(\theta_{31})]$, over quasilinear (QL) scales have yielded results which appear to agree loosely with the predictions of the so-called hierarchical model (Peebles 1975; Peebles 1980) for gravitational evolution of Gaussian initial conditions (Peebles & Groth 1975; Fry & Seldner 1982; Jing & Zhang 1989; Tóth, Hollósi, & Szalay 1989; Borgani, Jing, & Plionis 1992; Gaztañaga 1994; Bernardeau 1995; Cappi & Maurogordato 1995; Gaztañaga, Croft, & Dalton 1995; Gaztañaga & Bernardeau 1998; Jing & Börner 1998; Magliocchetti *et al.* 1998). It is obvious, however, that improved measurements [from surveys such as the Sloan Digital Sky Survey (SDSS; Loveday *et al.* 1998)] and more sophisticated theoretical modeling of angular CFs are required. In particular, there has been little theoretical work to date on the detailed behavior of angular CFs beyond the two-point function, despite the practical advantages they can offer.

In this paper, we present a calculation of the full angular 3PCF⁵, Z , as well as s_3 , for an arbitrary, biased, tracer-mass distribution in flat and open cold-dark-matter (CDM) models, assuming Gaussian initial conditions. The calculation, based on leading-order PT results, is restricted to the QL regime, where $\varpi \ll 1$, and further invokes the small-angle approximation. We take into account such factors as the explicit dependence on the cosmological parameters, the shape and linear evolution of the CDM power spectrum, and the form of redshift distribution function. We consider both the redshift distribution of the APM Galaxy Survey, as well as that of a survey with a mean redshift of $\bar{z} \simeq 1$. We also examine the effect of linear and nonlinear bias, which, through an extension of the Fry (1996) bias-evolution model to the case of an arbitrary expansion history, are allowed to evolve in time. Following BKJ, we define the bias parameters, b_i , by an expansion of the unsmoothed tracer-mass field in terms of the unsmoothed dark-matter field, rather than by relating the smoothed fields, as is often done (e.g., Fry & Gaztañaga 1993). While many of the results we obtain are similar to those found in a related paper (Buchalter & Kamionkowski 1999, hereafter BK99) dealing with the spatial 3PCF and skewness, understanding the detailed behavior of angular statistics in practice can be equally, if not more, illuminating. We extend previous derivations of s_3 (Bernardeau 1995) to include a scale-dependent, leading-order correction which arises in the case of nonlinear bias, as defined for the unsmoothed fields, and which becomes large for positive effective power-spectrum indices. This behavior, in principle, may allow better constraints on the linear- and nonlinear-bias parameters on the basis of large-scale skewness measurements alone, or at least differentiate between the smoothed and unsmoothed biasing scenarios. For plausible models, we find that s_3 is relatively insensitive to the adopted cosmology, as compared with its stronger dependence on the biasing scheme. In general, the presence of linear bias tends to flatten and reduce the scale dependence of s_3 , while a nonlinear bias tends to produce a relative increase. The full angular 3PCF, Z , shows similar sensitivities to the bias parameters, but can also depend significantly on the cosmological model, and in particular on the shape of the power spectrum. We find that the configuration dependence of Z is in general more complex than the simple hierarchical model suggests, and, since angular statistics probe clustering over a range of redshifts, is also sensitive to evolutionary effects. These properties can be used to discriminate between various models which can yield nearly degenerate predictions for s_3 , or for the spatial 3PCF at $z = 0$, such as evolving versus non-evolving bias models, or open versus flat cosmological models. Neglecting the full geometric and evolutionary variation of Z throws away valuable information which might, in practice, be harder to obtain from three-dimensional data. In several instances,

⁵Frieman & Gaztañaga (1999), using a different method, have independently derived results for Z . We have compared our results with theirs and find that they agree for some of the models we have considered.

we illustrate how accounting for time dependences in, e.g., the power spectrum or the bias, can impact the resulting calculations, especially in the case of high-redshift surveys. Our theoretical results, in general, should be comparable to current and future measurements of angular clustering.

In §2 we outline the calculations used and present results for the normalized angular skewness. In §3 we derive predictions for the full angular 3PCF and in §4 we summarize our conclusions. Since the calculations are greatly simplified by working initially in Fourier space, we first obtain the angular bispectrum—the two-dimensional projection of the spatial bispectrum—and then derive the angular 3PCF from this. A derivation of the equation that relates the spatial and angular bispectra is presented in the Appendix. This result is essentially a Fourier-space generalization of Limber’s equation for the 3PCF.

2. ANGULAR SKEWNESS

Since angular CFs involve projections of their full spatial counterparts, our derivations must involve integrals over the line of sight, which will in general depend on the adopted cosmological model. We shall consider open and flat Friedmann-Robertson-Walker (FRW) cosmologies with a possible cosmological constant, so that the scale factor, $a(t)$, satisfies the Friedmann equations,

$$\begin{aligned} \frac{\dot{a}}{a} = H_0 E(z) &\equiv H_0 \sqrt{\Omega_0(1+z)^3 + (1 - \Omega_0 - \Omega_\Lambda)(1+z)^2 + \Omega_\Lambda}, \\ \frac{\ddot{a}}{a} &= H_0^2 [\Omega_\Lambda - \Omega_0(1+z)^3/2], \end{aligned} \quad (1)$$

where Ω_0 is the present nonrelativistic matter density in units of the critical density, Ω_Λ is the contribution of the cosmological constant to the total present energy density, H_0 is the present value of the Hubble parameter, and a dot denotes a derivative with respect to time. The scale factor is chosen such that $a_0 H_0 = 2$, where $H_0 = 100 h \text{ km s}^{-1} \text{ Mpc}^{-1}$. If we take our position as the origin, $\mathbf{w} = 0$, then the angular-diameter distance to an object at redshift z is given by

$$w(z) = \frac{S(a_0 H_0 f(z) \sqrt{|1 - \Omega_0 - \Omega_\Lambda|})}{a_0 H_0 \sqrt{|1 - \Omega_0 - \Omega_\Lambda|}}; \quad f(z) = \frac{1}{2} \int_0^z \frac{dz'}{E(z')}, \quad (2)$$

where $S(x) = \{\sinh x, x, \sin x\}$, respectively, for open, flat, and closed geometries. For an Einstein-de Sitter universe, $w(z) = f(z)$. The distance to the horizon is given by $\eta_0 = w(\infty)$.

We wish ultimately to derive an expression for the angular 3PCF of a distribution of tracer masses (e.g., galaxies, quasars, clusters, radio sources, etc.), $Z(\theta_{12}, \theta_{23}, \theta_{31}) = \langle p(\boldsymbol{\theta}_1)p(\boldsymbol{\theta}_2)p(\boldsymbol{\theta}_3) \rangle$, where $\boldsymbol{\theta}$ represents two-dimensional coordinates on the sky, $p(\boldsymbol{\theta}) = [\Sigma(\boldsymbol{\theta}) - \bar{\Sigma}]/\bar{\Sigma}$ is the fractional perturbation to the unsmoothed tracer-mass density field, $\Sigma(\boldsymbol{\theta})$, and angular brackets denote an average over direction in the sky, with fixed values for the distances $\theta_{ij} = |\boldsymbol{\theta}_i - \boldsymbol{\theta}_j|$. Though statistical homogeneity and isotropy ensure that the 3PCF will only depend on the relative angular separations between the three points, measuring Z for all possible geometric configurations can nonetheless be a daunting task. For this reason, many studies have focussed instead on the normalized angular skewness, $s_3 \equiv \langle p_\Theta^3(\boldsymbol{\theta}) \rangle / \langle p_\Theta^2(\boldsymbol{\theta}) \rangle^2$, obtained from the moments of counts in cells smoothed with an effective angular scale half-width Θ (it is implicitly assumed that $\Sigma \propto n$, where n is the number of discrete counts). This one-point statistic is more readily calculable than the full angular 3PCF, while still preserving information about the overall scale-dependence of Z .

In deriving the following results, we implicitly make use of the small-angle approximation in assuming that a small patch of sky can be treated using a Fourier expansion (Peebles 1980). In this approximation, the component of the three-dimensional wave vector along the line of sight is taken to be negligible compared to the orthogonal components, so that the angular CFs depend only on the latter. We later comment on this assumption. We define p_Θ using a two-dimensional spherical top hat window function, so that in terms of the Fourier components, $\tilde{p}(\boldsymbol{\kappa})$, of the unsmoothed two-dimensional density field, we have

$$p_\Theta(\boldsymbol{\theta}) = \int \frac{d^2\boldsymbol{\kappa}}{(2\pi)^2} \tilde{p}(\boldsymbol{\kappa}) e^{i\boldsymbol{\kappa}\cdot\boldsymbol{\theta}} \mathcal{W}(\kappa\Theta), \quad (3)$$

where $\boldsymbol{\kappa}$ is a two-dimensional wave vector with magnitude κ , $\mathcal{W}(x) = 2J_1(x)/x$ is the Fourier transform of the two-dimensional spherical top-hat window function, and Θ is an angular smoothing radius. We can then obtain the angular 2PCF, as measured using counts in cells,

$$\varpi_\Theta(\theta_{12}) = \langle p_\Theta(\boldsymbol{\theta}_1)p_\Theta(\boldsymbol{\theta}_2) \rangle = \iint \frac{d^2\boldsymbol{\kappa}_1}{(2\pi)^2} \frac{d^2\boldsymbol{\kappa}_2}{(2\pi)^2} e^{i(\boldsymbol{\kappa}_1\cdot\boldsymbol{\theta}_1 + \boldsymbol{\kappa}_2\cdot\boldsymbol{\theta}_2)} \mathcal{W}(\kappa_1\Theta) \mathcal{W}(\kappa_2\Theta) \langle \tilde{p}(\boldsymbol{\kappa}_1)\tilde{p}(\boldsymbol{\kappa}_2) \rangle. \quad (4)$$

We define

$$\langle \tilde{p}(\boldsymbol{\kappa}_1)\tilde{p}(\boldsymbol{\kappa}_2) \rangle \equiv (2\pi)^2 \delta_D(\boldsymbol{\kappa}_1 + \boldsymbol{\kappa}_2) P_p(\kappa), \quad (5)$$

where the angular, or projected, power spectrum of the tracer mass, P_p (usually written in terms of C_ℓ 's in papers on the cosmic microwave background), can be related to the full tracer-mass power spectrum, $P(k, w)$, by a Fourier-space analog of Limber's equation

(Kaiser 1992),

$$P_p = \int_0^{\eta_0} \frac{dw}{w^2} \left(\frac{dN}{dw} \right)^2 P(\kappa/w, w). \quad (6)$$

Here, dN/dw is a w -space selection function for the tracer mass, normalized such that $\int_0^{\eta_0} dw (dN/dw) = 1$.

We assume the fractional perturbation to the *unsmoothed* three-dimensional tracer mass density field, $\delta(\mathbf{r})$, may be expanded in terms of the local perturbation to the unsmoothed, underlying matter field, $\delta_m(\mathbf{r})$, via

$$\delta = b_1 \delta_m + \frac{b_2}{2} \delta_m^2 + \dots, \quad (7)$$

where b_1 is the linear bias term, b_2 the first nonlinear term, etc., and δ_m is itself written as $\delta_m = \delta_m^{(1)} + \delta_m^{(2)} + \dots$, where $\delta_m^{(n)} \ll \delta_m^{(n-1)}$, $\delta_m^{(1)}$ is the linear solution, and $\delta_m^{(2)}$ characterizes the leading-order departure from the Gaussian initial conditions. The linear solution for the underlying spatial density contrast has the separable form

$$\delta_m^{(1)}(\mathbf{r}, w) = D(w) \delta_m^{(1)}(\mathbf{r}, 0), \quad (8)$$

so that fluctuations evolve simply as the linear growth factor, $D(w)$. This in turn implies that, to leading order, the spatial and time dependence of the power spectrum can likewise be factorized. For FRW cosmologies, the growth factor is given (as a function of redshift) by

$$D(z) = \frac{5\Omega_0 E(z)}{2} \int_z^\infty dz' \frac{1+z'}{[E(z')]^3}. \quad (9)$$

For an Einstein de-Sitter universe $D(w)$ is simply the scale factor, $a(w)$. Assuming the unsmoothed three-dimensional tracer-mass density contrast to be related to the underlying distribution via equation (7), we can write the leading-order result for the full linear power spectrum of the tracer mass,

$$P(k, w) = A b_1^2 D^2(w) k^n T^2(k), \quad (10)$$

where k^n is the primordial power spectrum, A is the overall amplitude, and $T(k)$ is a model-dependent transfer function. Substituting equations (10), (6), and (5) into (4), taking $\boldsymbol{\theta}_1 = \boldsymbol{\theta}_2 \equiv \boldsymbol{\theta}$, and $x = \kappa\Theta$, we arrive at the angular variance (the 2PCF at zero lag),

$$\varpi_\Theta(0) = \langle p_\Theta^2(\boldsymbol{\theta}) \rangle = \frac{A}{2\pi\Theta^{n+2}} \int_0^{\eta_0} dw \left(\frac{dN}{dw} \right)^2 \frac{b_1^2 D^2(w)}{w^{n+2}} \int_0^\infty dx x^{n+1} \mathcal{W}^2(x) T^2(x/\Theta w), \quad (11)$$

where the b_1 term is left inside the w integral to allow for the possibility of bias evolution.

The counts-in-cells angular 3PCF is given by

$$Z_{\Theta}(\theta_{12}, \theta_{23}, \theta_{31}) = \langle p_{\Theta}(\boldsymbol{\theta}_1) p_{\Theta}(\boldsymbol{\theta}_2) p_{\Theta}(\boldsymbol{\theta}_3) \rangle = \int \int \int \frac{d^2 \boldsymbol{\kappa}_1}{(2\pi)^2} \frac{d^2 \boldsymbol{\kappa}_2}{(2\pi)^2} \frac{d^2 \boldsymbol{\kappa}_3}{(2\pi)^2} e^{i(\boldsymbol{\kappa}_1 \cdot \boldsymbol{\theta}_1 + \boldsymbol{\kappa}_2 \cdot \boldsymbol{\theta}_2 + \boldsymbol{\kappa}_3 \cdot \boldsymbol{\theta}_3)} \\ \times \langle \tilde{p}(\boldsymbol{\kappa}_1) \tilde{p}(\boldsymbol{\kappa}_2) \tilde{p}(\boldsymbol{\kappa}_3) \rangle \mathcal{W}(\boldsymbol{\kappa}_1 \Theta) \mathcal{W}(\boldsymbol{\kappa}_2 \Theta) \mathcal{W}(\boldsymbol{\kappa}_3 \Theta). \quad (12)$$

The angular, or projected, bispectrum, B_p , is defined via

$$\langle \tilde{p}(\boldsymbol{\kappa}_1) \tilde{p}(\boldsymbol{\kappa}_2) \tilde{p}(\boldsymbol{\kappa}_3) \rangle \equiv (2\pi)^2 \delta_D(\boldsymbol{\kappa}_1 + \boldsymbol{\kappa}_2 + \boldsymbol{\kappa}_3) B_p(\boldsymbol{\kappa}_1, \boldsymbol{\kappa}_2, \boldsymbol{\kappa}_3), \quad (13)$$

and is related to the full three-dimensional bispectrum, B , by

$$B_p(\boldsymbol{\kappa}_1, \boldsymbol{\kappa}_2, \boldsymbol{\kappa}_3) = \int_0^{\eta_0} \frac{dw}{w^4} \left(\frac{dN}{dw} \right)^3 B(\boldsymbol{\kappa}_1/w, \boldsymbol{\kappa}_2/w, \boldsymbol{\kappa}_3/w, w) \quad (14)$$

(see Appendix). The full bispectrum is given, to leading order in PT, by

$$B(k_1, k_2, k_3, w) = P(k_1, w) P(k_2, w) \left\{ \frac{1}{b_1} \left[1 + \mu + \cos \psi \left(\frac{k_1}{k_2} + \frac{k_2}{k_1} \right) + (1 - \mu) \cos^2 \psi \right] \right. \\ \left. + \frac{b_2}{b_1^2} \right\} + (\text{cyc.}), \quad (15)$$

(Fry 1984; Goroff *et al.* 1986; Matarrese, Verde, & Heavens 1997) where ψ is the angle between \mathbf{k}_1 and \mathbf{k}_2 , and μ is a function of the expansion history, equal to 3/7 for an Einstein-de Sitter universe (Peebles 1980) and differing from this value only slightly for other reasonable choices of the density parameters (Bouchet *et al.* 1992; Bernardeau 1994; Bouchet *et al.* 1995; Catelan *et al.* 1995; Martel 1995; Scoccimarro *et al.* 1998; Kamionkowski & Buchalter 1998). Note that the expression for B includes the dependence on b_2 , since the leading-order result for the 3PCF includes second-order terms in the expansion of equation (7).

Evaluating equation (12) with $\boldsymbol{\theta}_1 = \boldsymbol{\theta}_2 = \boldsymbol{\theta}_3 \equiv \boldsymbol{\theta}$, $x_i = \kappa_i \Theta$, taking $\boldsymbol{\kappa}_1$ to lie in the $\psi = 0$ direction, and substituting equations (13), (14), and (15) we obtain, after a little algebra, an expression for the area-averaged skewness,

$$\langle p_{\Theta}^3(\boldsymbol{\theta}) \rangle = \frac{3A^2}{(2\pi)^3 \Theta^{2n+4}} \int_0^{\eta_0} dw \left(\frac{dN}{dw} \right)^3 \frac{b_1^4 D^4(w)}{w^{2n+4}} \\ \times \int_0^{\infty} dx_1 x_1^{n+1} \mathcal{W}(x_1) T^2(x_1/\Theta w) \int_0^{\infty} dx_2 x_2^{n+1} \mathcal{W}(x_2) T^2(x_2/\Theta w) \\ \times \int_0^{2\pi} d\phi \mathcal{W}(x_3) \left(\frac{1}{b_1} \left[(1 + \mu) + \cos \psi \left(\frac{x_1}{x_2} + \frac{x_2}{x_1} \right) + (1 - \mu) \cos^2 \psi \right] + \frac{b_2}{b_1^2} \right) \quad (16)$$

where one integral vanishes under the requirement $\kappa_3 = -(\kappa_1 + \kappa_2)$, and a factor of 3 arises from symmetry considerations applied to the 2 cyclic permutations in equation (15). Noting that $x_3 = \sqrt{x_1^2 + x_2^2 + 2x_1x_2 \cos \psi}$, we can evaluate the ψ integrals by using the summation theorems for Bessel functions (Gradshteyn & Ryzhik 1980; Bernardeau 1995) which yield:

$$\int_0^{2\pi} d\psi \sin^2 \psi \mathcal{W}(x_3) = \pi \mathcal{W}(x_1) \mathcal{W}(x_2), \quad (17)$$

$$\int_0^{2\pi} d\psi \left(1 + \frac{x_2}{x_1} \cos \psi\right) \mathcal{W}(x_3) = 2\pi J_0(x_2) \mathcal{W}(x_1), \quad (18)$$

$$\int_0^{2\pi} d\psi \mathcal{W}(x_3) = 2\pi \sum_{j=0}^{\infty} (2j+1) \mathcal{W}_{2j+1}(x_1) \mathcal{W}_{2j+1}(x_2), \quad (19)$$

where $\mathcal{W}_n(x) = 2J_n(x)/x$, so that $\mathcal{W}(x) = \mathcal{W}_1(x)$. Using the above results gives

$$\begin{aligned} \langle p_{\Theta}^3(\boldsymbol{\theta}) \rangle &= \frac{3A^2}{(2\pi)^2 \Theta^{2n+4}} \int_0^{n_0} dw \left(\frac{dN}{dw} \right)^3 \frac{b_1^4 D^4(w)}{w^{2n+4}} \\ &\int_0^{\infty} dx_1 x_1^{n+1} \mathcal{W}(x_1) T^2(x_1/\Theta w) \int_0^{\infty} dx_2 x_2^{n+1} \mathcal{W}(x_2) T^2(x_2/\Theta w) \\ &\left\{ \frac{1}{b_1} [J_0(x_2) \mathcal{W}(x_1) + J_0(x_1) \mathcal{W}(x_2)] - \frac{1}{2} \frac{(1-\mu)}{b_1} \mathcal{W}(x_1) \mathcal{W}(x_2) \right. \\ &\left. + \frac{b_2}{b_1^2} \sum_{j=0}^{\infty} (2j+1) \mathcal{W}_{2j+1}(x_1) \mathcal{W}_{2j+1}(x_2) \right\}. \end{aligned} \quad (20)$$

We re-emphasize that our results in general are based on leading-order PT and are thus restricted to the QL regime, i.e., scales large enough so that the rms density contrast fluctuations are small compared with unity. Numerical simulations and observations both confirm that higher-order nonlinear corrections have little impact on spatial statistics on QL scales (Szalay 1988; Tóth, Hollósi, & Szalay 1989; Gott, Gao, & Park 1991; Fry, Melott, & Shandarin 1993; Jain & Bertschinger 1994; Scoccimarro *et al.* 1998). By comparing with N -body results, Gaztañaga & Bernardeau (1998) test the validity of PT as applied to angular statistics and find good agreement on scales $\Theta \gtrsim 1^\circ$, with the details depending on the shape of the power spectrum. In addition, simulations show that QL scales can still obey leading-order PT even when smaller scales have become fully nonlinear (Bouchet & Hernquist 1992), and further that the predictions of QL PT may hold even on scales where the rms fluctuation exceeds unity (Bernardeau 1994; Baugh, Gaztañaga, & Efstathiou 1995; Fry, Melott, & Shandarin 1995; Szapudi *et al.* 1998).

Our results have also relied on the use of the small-angle approximation. The Fourier integrals used to calculate ϖ and Z , however, extend over all values of κ , including small values for which this approximation breaks down, but which nonetheless may

contribute significant weights to the integrands on degree scales.⁶ Moreover, the small-angle approximation might appear to go against the assumption of quasilinearity; in practice, the degree to which these two assumptions are mutually plausible will in general depend on the selection function in question. Despite these considerations, our results for s_3 and q on scales near 1° do agree well with data from observations (e.g., Gaztañaga 1994; see Figure 7) and N -body simulations (Frieman & Gaztañaga 1999) on these scales. Bernardeau (1995) investigates the validity of the small-angle approximation for models with different redshift selection functions, dN/dz , and finds good agreement with numerical results for s_3 on scales near and below 1° . Gaztañaga & Bernardeau (1998) find that the small-angle approximation can yield reasonable agreement with numerical results for s_3 out to the $5^\circ - 10^\circ$ scale. Verde *et al.* (1999) perform an exact calculation for the angular 3PCF using a spherical-harmonic decomposition, and a more complete comparison and assessment of the small-angle results against the exact results are presented therein.

2.1. Effects of the Power Spectrum

Equations (11) and (20) are one-point results which, for a given choice of Ω_0 , Ω_Λ , b_1 , and b_2 , depend only on the smoothing radius, Θ , and the form of the power spectrum. If we assume, for computational simplicity, a scale-free power spectrum, $P(k) \propto k^n$ [$T(k) = 1$], then we can calculate an expression for s_3 where the x integrals can be separated from the w integration and evaluated analytically; combining equations (11) and (20), we obtain

$$s_3 = \frac{\langle p_\Theta^3(\boldsymbol{\theta}) \rangle}{\langle p_\Theta^2(\boldsymbol{\theta}) \rangle^2} = R_3(n) \left\{ \frac{1}{b_1} \left[\frac{36}{7} + \frac{9}{14} \left(\frac{7}{3}\mu - 1 \right) - \frac{3}{2}(n+2) \right] + 3 \frac{b_2}{b_1^2} [1 + \Delta(n)] \right\}, \quad (21)$$

where

$$R_3(n) = \frac{\int_0^{\eta_0} dw (dN/dw)^3 w^{-(2n+4)} D^4(w)}{\left[\int_0^{\eta_0} dw (dN/dw)^2 w^{-(n+2)} D^2(w) \right]^2}, \quad (22)$$

and

$$\Delta(n) = \frac{\sum_{j=1}^{\infty} (2j+1) \left[\int_0^{\infty} dx x^{n-1} J_1(x) J_{2j+1}(x) \right]^2}{\left[\int_0^{\infty} dx x^{n-1} J_1^2(x) \right]^2}. \quad (23)$$

Note that while the term in curly brackets in equation (21) depends only very weakly on Ω_0 through μ , the $R_3(n)$ term depends on the cosmological model both through the presence of the linear growth factor, D (which is often neglected), as well as through the explicit dependence of w on the expansion history [see equation (2)]. Equations (21)–(23)

⁶We note that this difficulty could be avoided if one considers the bispectrum directly.

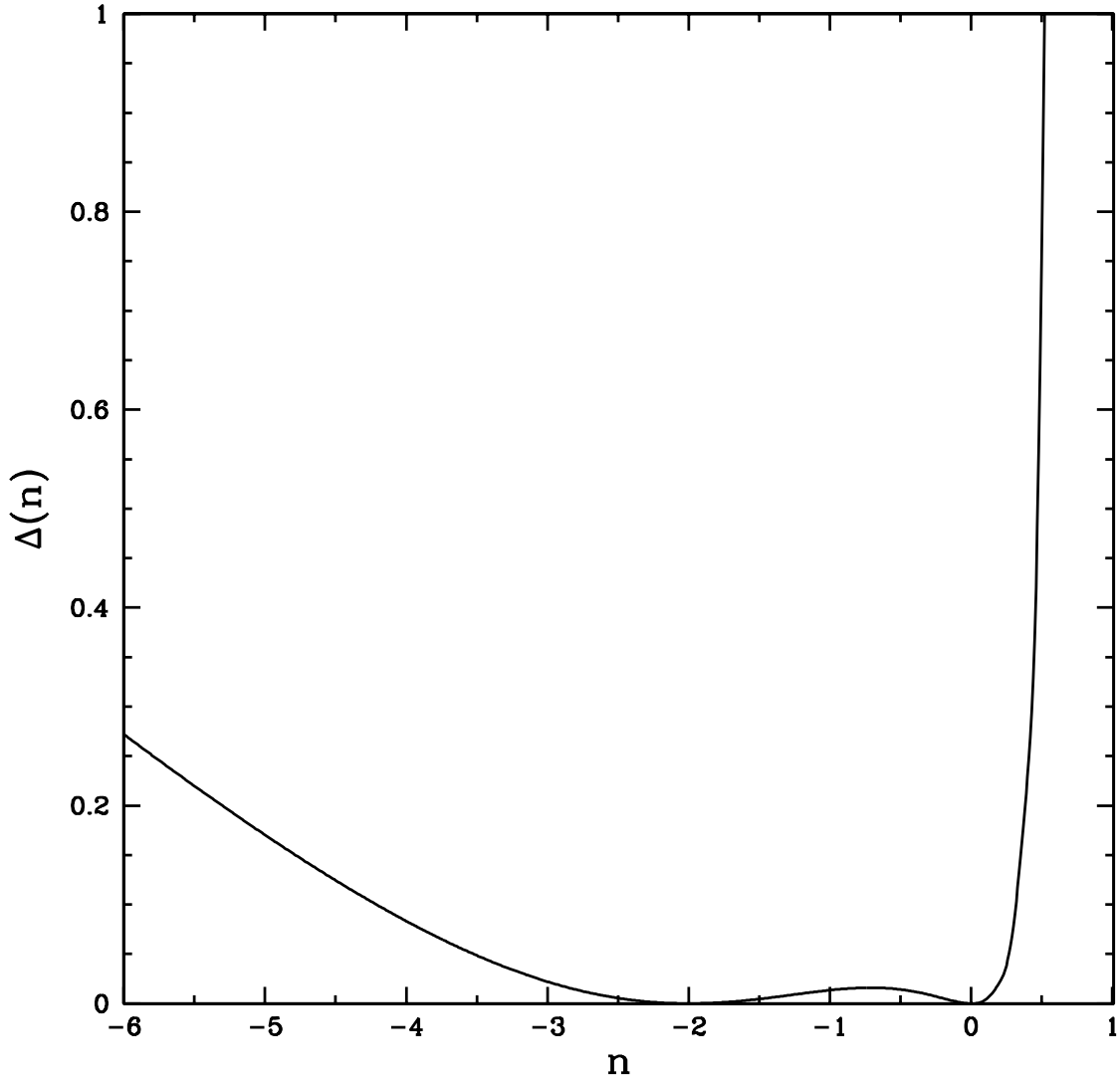


Fig. 1.— The variation of the Δ term in equation (21) with spectral index n . Though negligible for n in the range $-2 < n < 0$, this term rapidly becomes significant for $n > 0$, due to the impact of small-scale fluctuations.

are valid for n in the range $-2 > n > 1$; the individual terms in the series for $\Delta(n)$ can be evaluated explicitly (Watson 1966) and we find that $\Delta(n) \ll 1$ for $-2 < n < 0$, but diverges for $n > 0$, as illustrated in Figure 1.

The bracketed n -dependent terms in equation (21) arise from the effects of smoothing the contiguous field, $\delta(\mathbf{r})$, defined in equation (7). In particular, since smoothing at a fixed physical mixes different mass scales, the higher-order moments for smoothed fields will generally contain additional terms reflecting the scale dependence of the rms fluctuation (Bernardeau 1994, 1995). The $n = -2$ case thus recovers the no-smoothing result for s_3 (Bernardeau 1995), since the rms fluctuation in this case is independent of scale [see equation (11)]. Though the filter is designed to separate out the nonlinear, small-scale fluctuations, an unbounded scale-free power spectrum with $n > 0$ produces so much small-scale power that the fluctuations induced by smoothing over nonlinear scales become comparable to or greater than the large-scale linear perturbations, leading to the divergence in $\Delta(n)$ seen in the Figure.

Equation (21) differs from the known result for s_3 assuming constant, nonlinear bias (Bernardeau 1995) only in that it contains the $\Delta(n)$ term. The difference is attributable to the fact that previous authors usually define the bias parameters using the form of equation (7), but relating the *smoothed*, rather than the unsmoothed, observed and underlying density fields. Such a definition is technically nonlocal, only fixing the linear- and nonlinear-bias parameters at the chosen smoothing scale. While it can be shown that the “smoothed” and “unsmoothed” linear-bias parameters are identical, the value of the smoothed nonlinear-bias parameter will, unlike the unsmoothed b_2 defined in equation (7) in the limit of continuous fields, depend on the smoothing scale. Comparing the result for s_3 with those of Fry & Gaztañaga (1993) and Bernardeau (1995), we can infer that the smoothed nonlinear-bias parameter will vary as $b_2[1 + \Delta(n)]$. In the limit of no smoothing ($n = -2$), the two parameters are identical, as expected, but can differ dramatically on large scales (see §2.2). Similar correction terms, arising from nonlinear bias, are expected for higher-order angular moments as well. Such terms might be used to discriminate between the smoothed and unsmoothed bias pictures, and possibly distinguish between linear and nonlinear bias based on the skewness alone, as discussed in §2.2 and in BK99. Unless stated otherwise, it will be hereafter understood that “bias” shall refer to the unsmoothed bias prescription defined by equation (7).

While the power spectrum for any viable cosmological model will not be given by a simple power law, it can be shown, using the results of Bernardeau (1995) and Gaztañaga & Bernardeau (1998), that an exact result for s_3 can be obtained for arbitrary power spectra, using a properly redefined *effective* index (Scoccimarro 1998). This result, analogous to

that in the spatial case (Bernardeau 1994), is strictly valid, however, only for linear biasing, since it fails to account for the above-mentioned large-scale variation associated with b_2 . Since we wish to consider nonlinear biasing, and because, unlike s_3 , no corresponding exact result can be obtained for the full angular 3PCF in the case of arbitrary power spectra, even for linear biasing, the results of this paper are based entirely on numerical integration of the appropriate equations. Many of these will involve highly oscillatory integrands, making them difficult to evaluate; we have performed checks on the numerical accuracy of our results, and found them to be good to within a few percent.

For realistic CDM models, we employ a transfer function given by

$$T(q) = \frac{\ln(1 + 2.34q)/(2.34q)}{[1 + 3.89q + (16.1q)^2 + (5.46q)^3 + (6.71q)^4]^{1/4}} \quad (24)$$

(Bardeen *et al.* 1986), where $q = k_p/\Gamma$, $\Gamma \approx \Omega_0 h$, and k_p is the physical wavenumber in units of $h \text{ Mpc}^{-1}$, related to the comoving wavenumber, k , through our adopted normalizations by $k_p = k/6000 h \text{ Mpc}^{-1}$. The result for s_3 is then obtained by using equation (24) together with (11) and (20). Note that in the case of a scale-dependent transfer function the x and w integrals cannot be separated.

Our calculations also require the assumption of a selection function (SF) along the line of sight, and we consider two functional forms chosen to characterize low-redshift ($\bar{z} \sim 0.1$) and high-redshift surveys ($\bar{z} \sim 1$). For the former, we consider the SF of the Automatic Plate Measuring (APM) Galaxy Survey,

$$\frac{dN}{dz} \propto z^2 \exp \left[- \left(\frac{z}{z_c} \right)^{3/2} \right]; \quad z_m = 1.412z_c, \quad (25)$$

where z_m is the median redshift of the survey, taken to be 0.12. This functional form provides very good fit to the APM redshift distribution over the entire APM magnitude range (Baugh & Efstathiou 1993; Maddox, Efstathiou, & Sutherland 1996; Gaztañaga & Baugh 1998), and should also approximate comparable optical surveys, such as the SDSS. To compare the expected results for a survey such as the APM, which reaches only modest redshifts ($z < 0.4$), with those from a much deeper angular survey, we also employ the w -space SF of Kaiser (1992) (intended to mimic a magnitude-limited survey),

$$\frac{dN}{dw} = \frac{\beta w^\alpha \exp \left[-(w/w_*)^\beta \right]}{w_*^{1+\alpha} \Gamma [(1+\alpha)/\beta]}; \quad w_* = \bar{w} (\Gamma [(2+\alpha)/\beta] \Gamma [(1+\alpha)/\beta]), \quad (26)$$

where \bar{w} is the mean conformal lookback time. We will hereafter choose $\alpha = 4$, $\beta = 4$, and $\bar{w} = 0.35$, which yields a peak redshift of $z \sim 0.8$, so that this model, which we will refer to as the “high- z ” SF, might characterize, for example, a radio survey such as the VLA

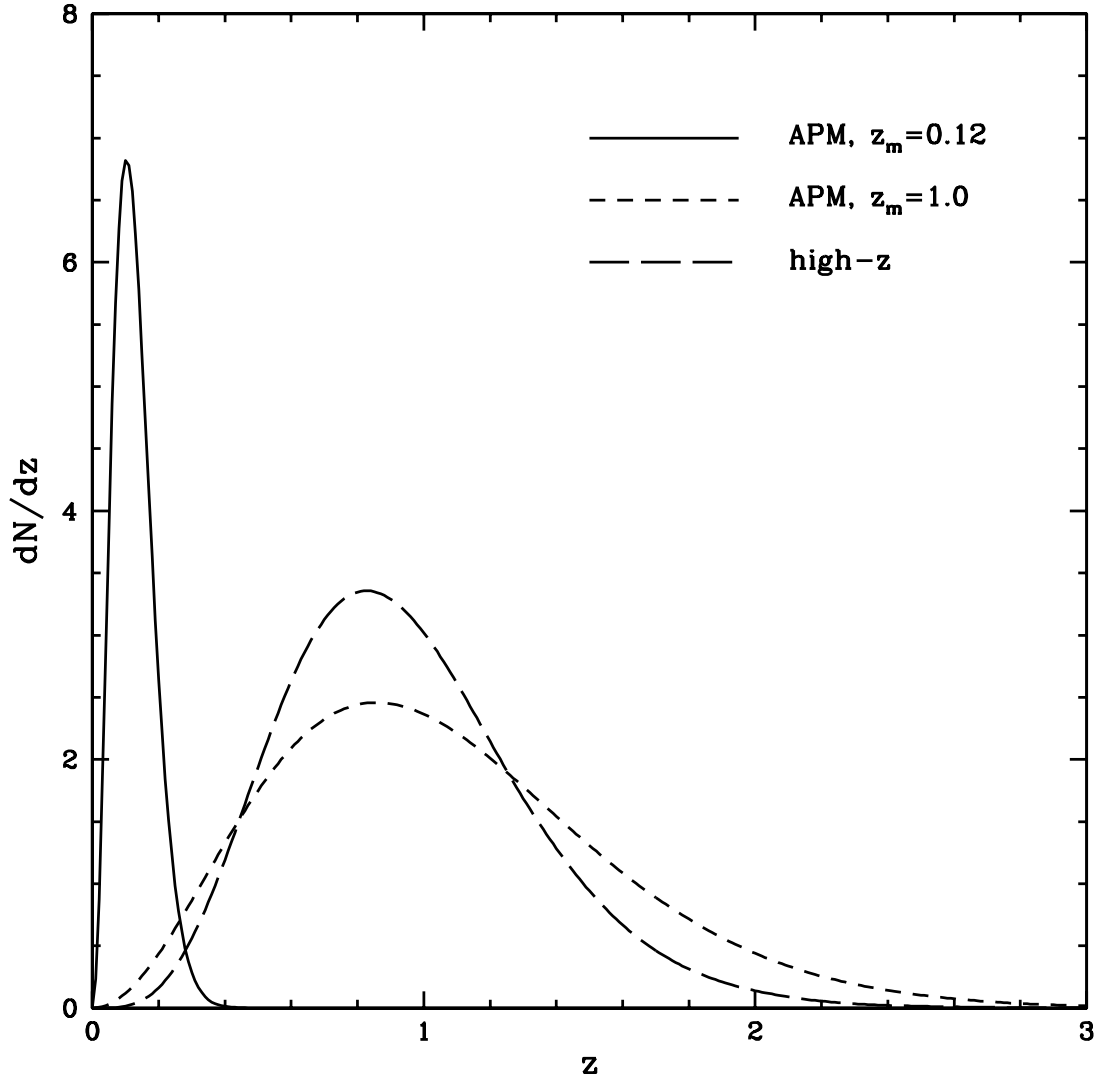


Fig. 2.— Redshift-space plot of the APM ($z_m = 0.12$) and high- z ($\bar{z} \simeq 1$) selection functions employed in the calculations. For comparison, we also display the APM SF assuming $z_m = 1.0$; both this and the high- z SF have been assigned three times the normalization of the low-redshift APM SF for the purposes of representation.

FIRST Survey (Becker, White, & Helfand 1995), with a median redshift of $z_m \sim 1$ (Cress & Kamionkowski 1998). Figure 2 shows the above APM SF together with the high- z SF, as well as the APM SF obtained using $z_m = 1.0$, for comparison. Baugh & Efstathiou (1993) and Maddox, Efstathiou & Sutherland (1996) find that angular statistics in the APM Survey depend much more sensitively on the peak redshift of the SF, rather than on its precise shape; we find this conclusion to hold in general for SFs we consider. Bernardeau (1995) finds that the small-angle approximation works reasonably well for an APM-like SF; for deeper surveys in which a fixed angle can probe larger scales, this approximation is expected to provide still better results.

In Figure 3, we plot the variation of s_3 with Θ , assuming the APM SF, for an unbiased ($b_1 = 1, b_2 = 0$) tracer-mass population in four flat ($\Omega_0 + \Omega_\Lambda = 1$) cosmological models: standard CDM (SCDM; $\Omega_0 = 1, h = 0.5, n = 1$), a tilted CDM model (TCDM; $\Omega_0 = 1, h = 0.5, n = 0.8$), CDM with a cosmological constant (Λ CDM; $\Omega_0 = 0.4, h = 0.5, n = 1$), and CDM with a high Hubble parameter (HCDM; $\Omega_0 = 1, h = 0.75, n = 1$), as well as an open CDM model (OCDM; $\Omega_0 = 0.4, h = 0.5, n = 1$). The thin horizontal line in the Figure shows the (virtually Ω_0 -independent) semi-analytic results obtained for a scale-free power spectrum with a canonical index value of $n = -1.2$ (Peebles 1980). The results for s_3 in general are very similar to those found by BK99 for the normalized spatial skewness. The scale-dependent CDM transfer function naturally induces a dependence on the smoothing scale, Θ , and compared to equation (21), a more substantial dependence on the combination of cosmological parameters $\Gamma = \Omega_0 h$. Yet, although the five cosmological models shown in the Figure span a broad range of parameter values, $0.2 < \Gamma < 0.75$, they yield fairly similar results, and are certainly all consistent within the limits of current observations (see Figure 7). The slight variation seen is mostly due to the dependence on Γ ; there is little difference between the SCDM and TCDM models, which differ only in the value of n , and virtually no difference between the OCDM and Λ CDM models. If the analysis is restricted to the range $0.2 < \Gamma < 0.3$, as suggested by current data (Bartlett *et al.* 1998), one can infer from the Figure that the predicted values for s_3 for a survey such as the APM are relatively insensitive to the adopted cosmological model. Figure 4 shows the results for $s_3(\Theta)$ for the same five cosmological models, assuming the high- z SF. The primary dependence is again seen to be with Γ , and while there is a somewhat greater spread between the different models, the differences between realistically viable models are still relatively small compared to those induced by the bias dependences which we explore in the next section.

Overall, we find that the high- z SF curves for these models show greater variation of s_3 with Θ than their APM SF counterparts. This is simply due to the fact that in a deeper angular survey, a fixed angle probes clustering over a broader range of physical scales, including very large scales, while conversely, in a shallower survey, a fixed angle

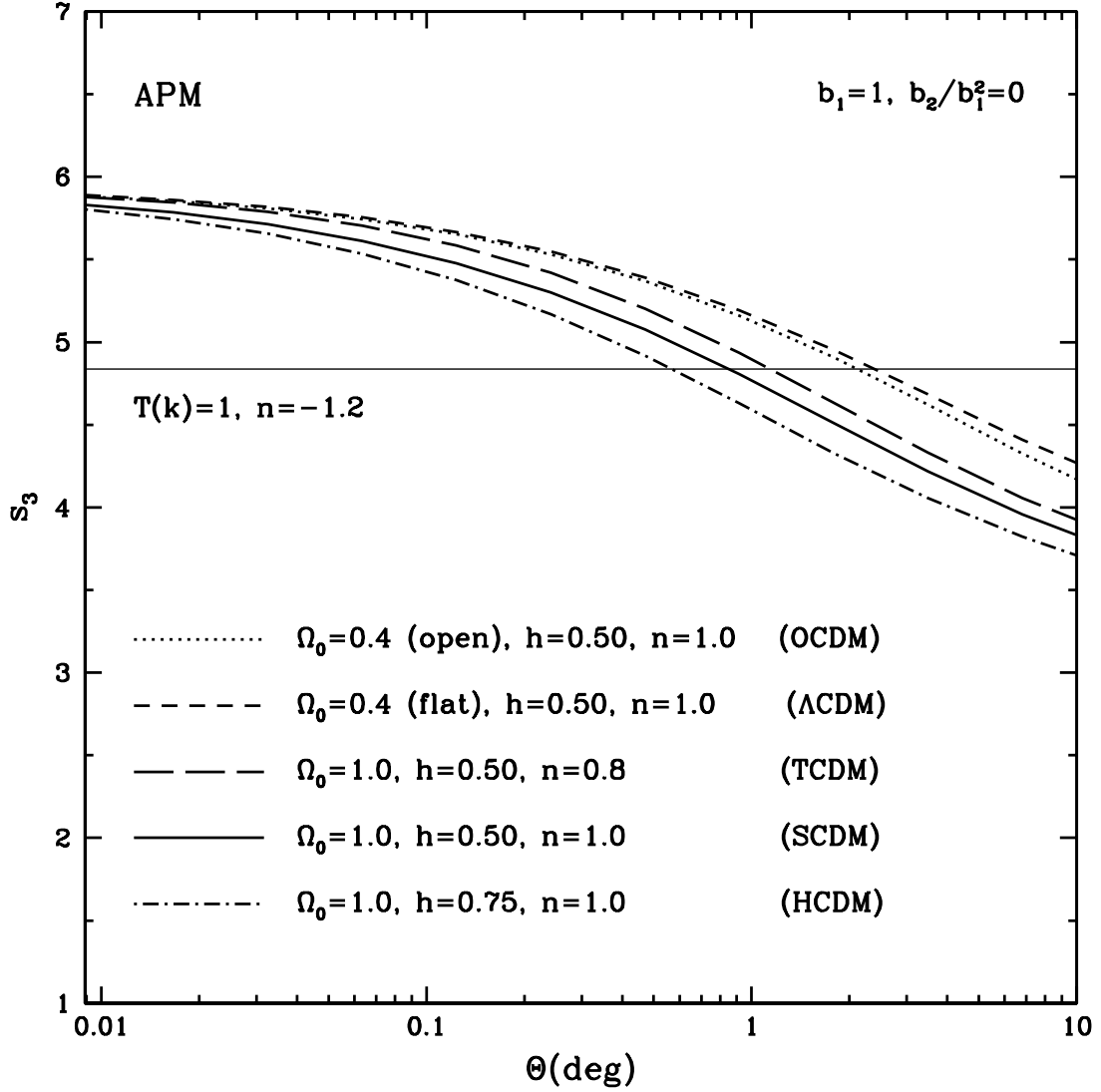


Fig. 3.— The variation of s_3 with Θ , for the APM SF, in the five cosmological models described in the text, assuming no bias. Note that the differences between these models are relatively small. The large values of s_3 at high Θ are due to the shallowness of the SF. The solid, horizontal line shows the result obtained from equation (21) for a scale-free power spectrum with $n = -1.2$.

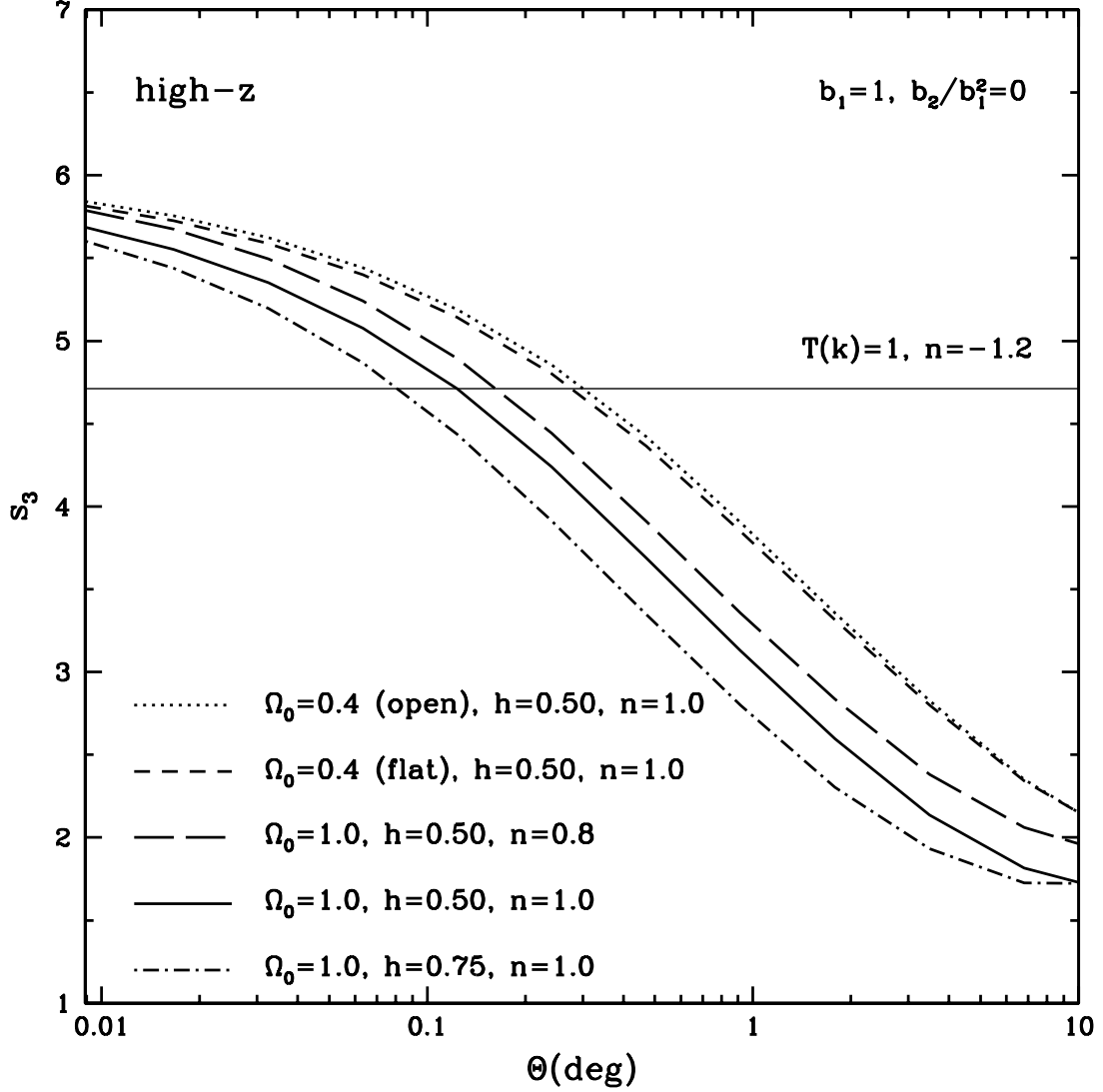


Fig. 4.— Same as Figure 3, but using the high- z SF. The models differ slightly more than in the APM case, and attain smaller values of s_3 at high Θ since these angular scales, in a deeper survey, incorporate larger physical scales where the effective power-spectrum index is larger.

is sensitive to clustering only over a relatively narrow range of smaller physical scales. Thus, at larger values of Θ , the high- z result incorporates physically large scales and tends toward smaller values for s_3 . These can be roughly approximated using equation (21) by $s_3 \approx R_3(n_k) \times [36/7 - (3/2)(n_k + 2)] \approx R_3(n_k) \times (9/14)$, where n_k , the value of the effective spectral index of the (untilted) linear-theory CDM power spectrum, tends towards unity at large scales (recall that R_3 is of order unity and independent of Θ). For the APM case, however, s_3 remains higher at larger Θ , since even large angular scales in a shallower survey still correspond only to smaller physical scales, where the effective power-spectrum index is negative. At smaller Θ , both sets of curves tend toward the expected larger values of $s_3 \approx R_3(n_k) \times (93/14)$ obtained with $n_k \approx -3$ —the effective power-spectrum index at small scales; for tilted models, s_3 tends toward a value $n_k - 1$ smaller. Note that in both Figures, the semi-analytic results for a scale-free power spectrum with a canonical index value of $n = -1.2$ (thin, horizontal lines) provide poor fits to the CDM predictions. Other authors have investigated QL results for the normalized angular skewness using CDM models (Gaztañaga & Frieman 1994; Frieman & Gaztañaga 1994; Gaztañaga & Baugh 1998; Gaztañaga & Bernardeau 1998), and find similar results.

2.2. The Effects of Bias and its Evolution

The results of the previous section already allow for the existence of a constant, nonlinear bias between the tracer-mass and the underlying matter distributions, but can be generalized by allowing the bias parameters to evolve with time, as is suggested both by theory and observations (Fry 1996; Peacock 1997; Matarrese *et al.* 1997; Steidel *et al.* 1998; Cress & Kamionkowski 1998; Catelan *et al.* 1998; Taruya, Koyama, & Soda 1998; Tegmark & Peebles 1998; Colín *et al.* 1998; Baugh *et al.* 1998; Magliocchetti & Maddox 1998). Fry (1996) proposes a bias-evolution model, which assumes that objects in an Einstein-de Sitter universe form at a fixed formation redshift, z_f , by some arbitrary local process which induces a bias at that epoch, and are subsequently governed purely by gravity. We note that this model fails to account for merging, and cannot produce an anti-bias ($b_1 < 1$). BK99 discuss a generalization of the Fry model to the case of arbitrary expansion history. Other, more general models have been proposed (e.g., Tegmark & Peebles 1998), but we employ the generalized Fry model as a first approximation to investigate the effects of bias evolution, and merely quote the relevant results below. The bispectrum in this model is given by

$$\begin{aligned}
 B(k_1, k_2, k_3, w) &= P(k_1, w)P(k_2, w) \left[C_1(w) + C_2(w) \cos \psi \left(\frac{k_1}{k_2} + \frac{k_2}{k_1} \right) + C_3(w) \cos^2 \psi \right] \\
 &+ (\text{cyc.}), \tag{27}
 \end{aligned}$$

where

$$C_1(w) = \frac{(10/7)d^2(w) + 2(b_{1*} - 1)[d(w) - 2/7] + b_{2*}}{[d(w) + b_{1*} - 1]^2}, \quad (28)$$

$$C_2(w) = \frac{d(w)}{d(w) + b_{1*} - 1}, \quad (29)$$

$$C_3(w) = \frac{(4/7)[d^2(w) + b_{1*} - 1]}{[d(w) + b_{1*} - 1]^2}, \quad (30)$$

$d(w) = D(w)/D(w_*)$, and a subscripted asterisk denotes the value of that parameter at the epoch of formation. Note that we have now ignored the very weak dependence of the bispectrum on μ ; the dependence on the expansion history, i.e., on the species contributing to the total energy density, is contained in the growth factor, $D(w)$. The result for s_3 can then be extended to the case of evolving bias by using the bispectrum of equation (27) in equation (16), which amounts to making the substitutions

$$\frac{1}{b_1} \longrightarrow C_2(w), \quad \frac{(1-\mu)}{b_1} \longrightarrow C_3(w), \quad \frac{b_2}{b_1^2} \longrightarrow C_1(w) - 2C_2(w) + C_3(w) \quad (31)$$

inside the brackets in equation (20), and replacing b_1 by $1/C_2(w)$.

For the APM and high- z SFs, respectively, Figures 5 and 6 display the results for $s_3(\Theta)$ in five different bias scenarios, each employing the SCDM, Λ CDM, and OCDM models above: an unbiased scenario ($b_1 = 1$, $b_2/b_1^2 = 0$, taken from Figures 3 and 4), a non-evolving, linear bias ($b_1 = 2$, $b_2/b_1^2 = 0$), a non-evolving, nonlinear bias ($b_1 = 2$, $b_2/b_1^2 = 1$), an evolving, linear bias ($b_{1*} = 5$, $b_{2*}/b_{1*}^2 = 0$), and an evolving, nonlinear bias ($b_{1*} = 5$, $b_{2*}/b_{1*}^2 = 1$). For the non-evolving bias scenarios, the Λ CDM and OCDM models are taken to be identical, as suggested by Figures 3 and 4, and therefore only the Λ CDM models are plotted in these cases. These two models do, however, differ slightly more in evolving bias scenarios, due to the different time dependences of their linear growth factors, and the differences between them would increase with decreasing Ω_0 . For the evolving cases we hereafter assume a formation redshift of $z_f = 5$.

The qualitative dependences of s_3 on the bias scenario are similar to those of its spatial counterpart (BK99). Specifically, it is clear from these Figures that the dependence of the angular skewness on the biasing scheme can potentially be far more significant than that upon the cosmological parameters within a given scheme. For example, adding a very small linear bias to the low- Γ models would yield a result very similar to the unbiased SCDM predictions. Generally, the presence of any significant linear bias, $b_1 > 1$, tends to reduce the dependence of s_3 on Θ , as compared with the unbiased cases (solid lines). Furthermore, an observed s_3 curve which is far below the predicted unbiased result can only be achieved

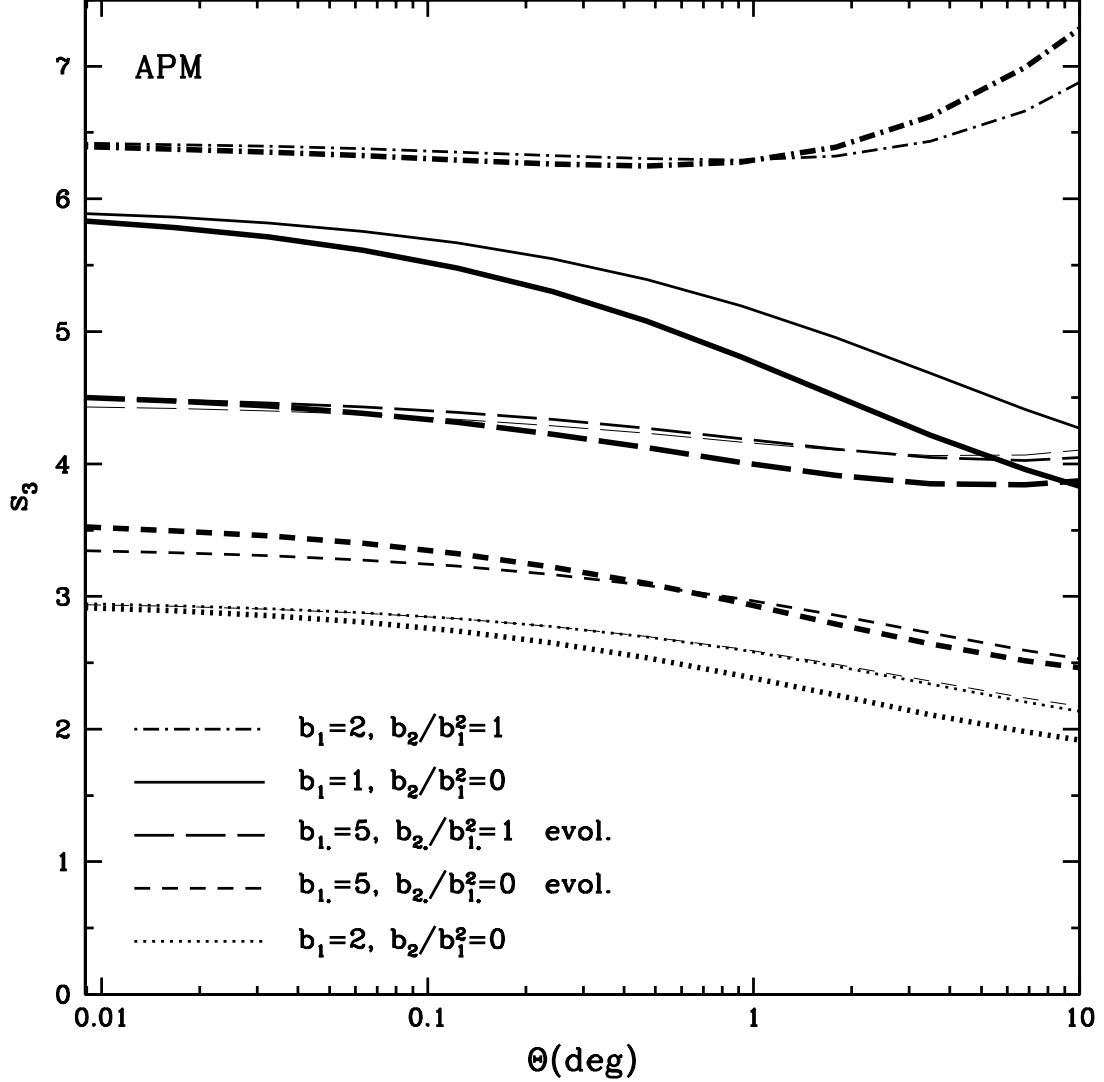


Fig. 5.— Plot of $s_3(\Theta)$, assuming the APM SF, for the five bias scenarios described in the text, each employing the SCDM model (thick lines), Λ CDM model (medium lines), and OCDM model (thin lines). For the non-evolving bias cases, the latter two models are taken to be identical, as suggested by Figure 3. Note the strong sensitivity to the biasing scheme and the presence of the upturn in s_3 at large Θ in the nonlinear bias cases. As expected, linear biasing tends to lower the predicted curves, while nonlinear biasing tends to raise them. The evolving bias models yield less dramatic shifts than their non-evolving counterparts, since evolving bias can effectively act as a constant bias, which at late times will be small.

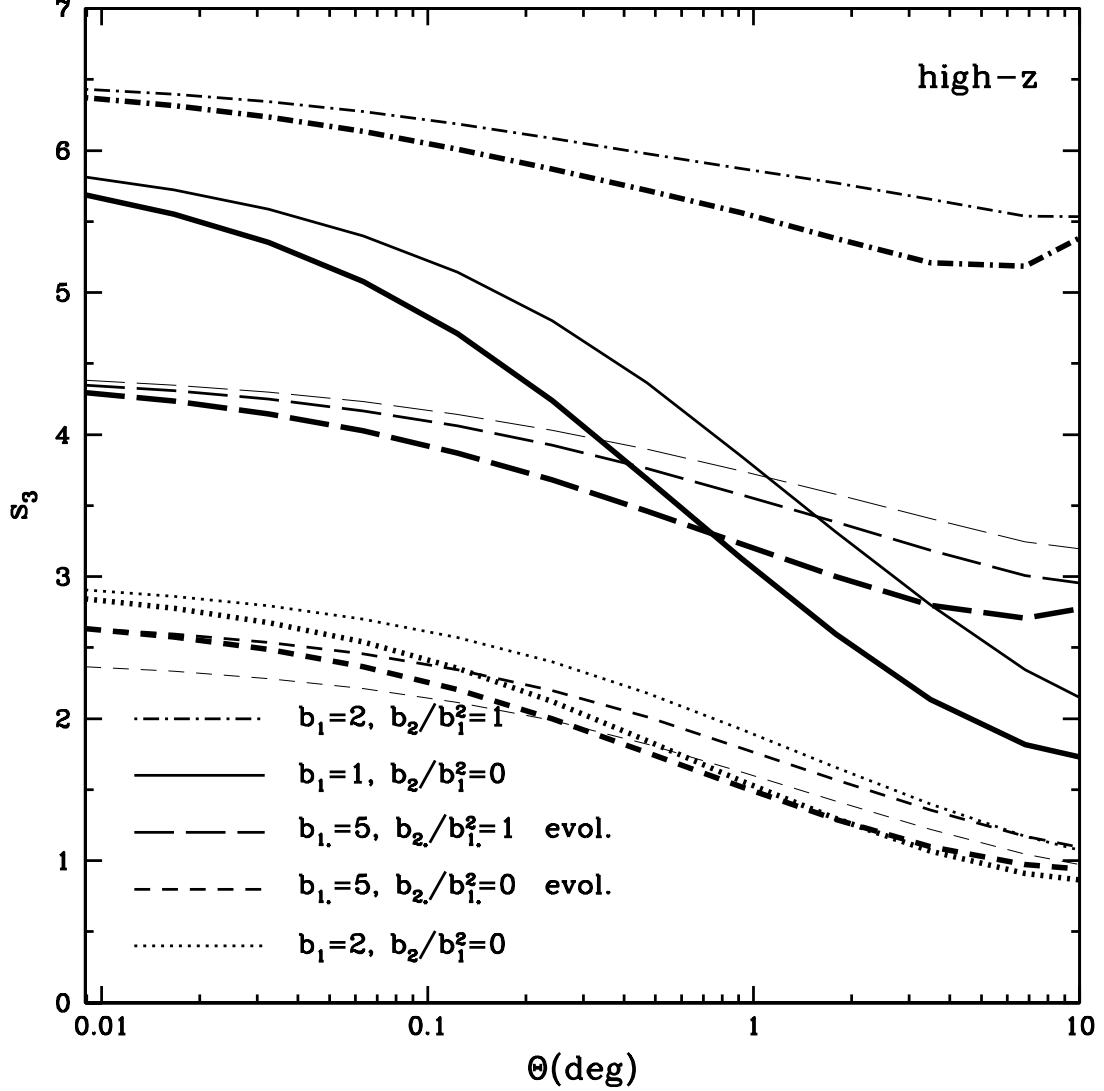


Fig. 6.— Same as Figure 5, but using the high- z SF. Note again the impact of the biasing scheme, the signatures of linear and nonlinear biasing, and the upturn in s_3 seen in cases where $b_2 \neq 0$. The Figure also illustrates one example of the possible degeneracies of s_3 with respect to the cosmological parameters, the bias parameters, and the evolution in the latter. In this case, the predictions for the SCDM and Λ CDM models with evolving linear-bias ($b_{1*} = 5$; short-dashed lines) are respectively similar to the SCDM and Λ CDM/OCDM models with constant, linear bias ($b_1 = 2$; dotted lines).

by a large linear bias term (assuming $b_2 \geq 0$), while one well above this value can only arise from the existence of a non-zero b_2 term or from anti-biasing ($b_1 < 1$). The curves for an evolving bias can produce less drastic shifts than their non-evolving counterparts, despite the fact that the respective bias terms are initially larger. This is because the evolution towards an unbiased state can effectively mimic a smaller (especially at late times), constant bias, as demonstrated by BK99.

Again we find that the APM curves in Figure 5 are flatter than their high- z counterparts in Figure 6, for reasons explained in §2.1. Note also that models with nonlinear bias exhibit an upturn at large Θ . The upturn arises from the contribution of the higher-order terms in the sum in equation (20), which, in the presence of a non-zero b_2 term, can become significant on large scales, where the effective power-spectrum index becomes positive (see Figure 1). BK99 perform the analogous three-dimensional calculation and find similar large-scale behavior of the normalized spatial skewness, S_3 . Depending on the cosmological model, this transition here occurs at angular scales of about a few degrees for the APM SF, and slightly higher values in the case of the high- z SF. Thus, the SCDM model, whose power spectrum peaks at larger wavenumber than those of the low- Γ models, will exhibit the upturn at smaller values of Θ , while the low- Γ models with nonlinear bias are expected to show an upturn only at larger angular scales, where they begin to sample positively-sloped regions of the power spectrum. However, unlike the case for S_3 (BK99), the exact location and severity of this upturn in s_3 for the different cosmological models is influenced not only by the shape of the power spectrum, but also by the weightings arising from the SF (see Figure 2) and from the terms proportional to powers of w in equations (20) and (11). For example, the APM SF, which resembles a low- w spike, exacerbates the upturn by effectively sampling the w integrals only around the low peak value of $w(z_m)$, where the $w^{-(2n+4)}$ factor is extremely large. In the case of the high- z SF, while large values of Θ still sample a positively-sloped region of $P(k)$, the SF itself, which is everywhere much shallower than in the APM case, is effectively zero where the $w^{-(2n+4)}$ factor is large, and peaks at a high value of w , where this factor is very small. As seen in Figure 6, this behavior tends to lend less support to the divergence of the sum in equation (20) at these scales, even in the case of a large, constant value of b_2 . Note that for both SFs, the non-evolving, nonlinear cases exhibit more of an upturn, since in these cases the large value of b_2 is maintained for all time, whereas in the evolving cases, the divergence is less severe due to the fact that the tracer population evolves towards an unbiased state with time.

The upturn in s_3 at large Θ in nonlinear-bias models differs from the decreasing behavior expected if the higher-order terms in the sum in equation (20) are neglected, i.e., if the bias parameters, as defined for *smoothed* density fields in equation (7), are assumed to be constant, as in peak-biasing or halo-biasing models (Mo & White 1996). BK99 show in

the case of the normalized spatial skewness that this different large-scale behavior might be used to obtain better constraints on b_1 and b_2 on the basis of skewness measurements alone, since combinations of linear and nonlinear bias which yield effectively degenerate results for S_3 on smaller smoothing scales, can, at least in principle, be distinguished by considering smoothing scales where the relevant *effective* index (Bernardeau 1994) is positive, i.e., scales greater than $100 h^{-1}$ Mpc in typical CDM models (see Figures 2 and 5 in BK99 and related discussions). Similarly, we can infer from Figures 5 and 6 that combinations of these parameters which are degenerate at small Θ become more distinct at large Θ (due to the upturn), and that comparing QL PT predictions with large-scale measurements ($\Theta \gtrsim 5^\circ$) of s_3 might also resolve this degeneracy. If this large-scale behavior is not seen, this would argue in favor of smoothed-bias prescriptions, rather than the unsmoothed formulation we employ. At such scales, however, one might be limited by the variance induced from the smaller number of independently sampled cells (Seto & Yokoyama 1998), and may require a more accurate derivation which does not assume the small-angle approximation, but instead employs a full spherical harmonic decomposition (Verde *et al.* 1999).

Figures 5 and 6 also provide illustrations of one of the potential degeneracies that can arise when considering the normalized skewness. It is known that the one-point statistics S_3 and s_3 can be nearly degenerate with respect to combinations of cosmological and biasing models, with respect to constant b_1 and b_2 (barring large-scale measurements, as mentioned above), and also with respect to evolving vs. non-evolving bias models (BK99). This latter degeneracy is illustrated in Figure 5 by the almost identical predictions of the OCDM model with evolving, linear bias and the OCDM/ Λ CDM model with constant, linear bias, and in Figure 6 by the similarity between the SCDM models with constant, linear bias and with evolving, linear bias. It would clearly be impossible to distinguish between such similar predictions given present data of the type shown in Figure 7.

As an example of what can be learned from current measurements, we compare in Figure 7 our predictions for s_3 using the APM SF with data from the APM Galaxy Survey, containing over 1.3×10^6 galaxies (see Gaztañaga 1994 and references therein). The data points (Gaztañaga 1997) are not corrected for the effects of source fragmentation, and the error bars shown are derived from the scatter in four sub-zones, plus shot-noise corrections, and are thus extremely conservative, especially at large Θ . The curves plotted are for the SCDM and Λ CDM models, with “best-fit” values for b_1 of 1.14 and 1.22, respectively (assuming only constant, linear biasing). It should be noted that discrepancies between the data and our QL PT predictions are expected at small scales, due to: 1) shot-noise fluctuations arising from the discreteness of the observed distribution [i.e., the $\langle p_\Theta^j \rangle$ are no longer reliable estimators of the area-averaged CFs (Peebles 1980; Gaztañaga 1994, 1997)], 2) estimation biases arising from the fact that the ratio of two unbiased estimators is not

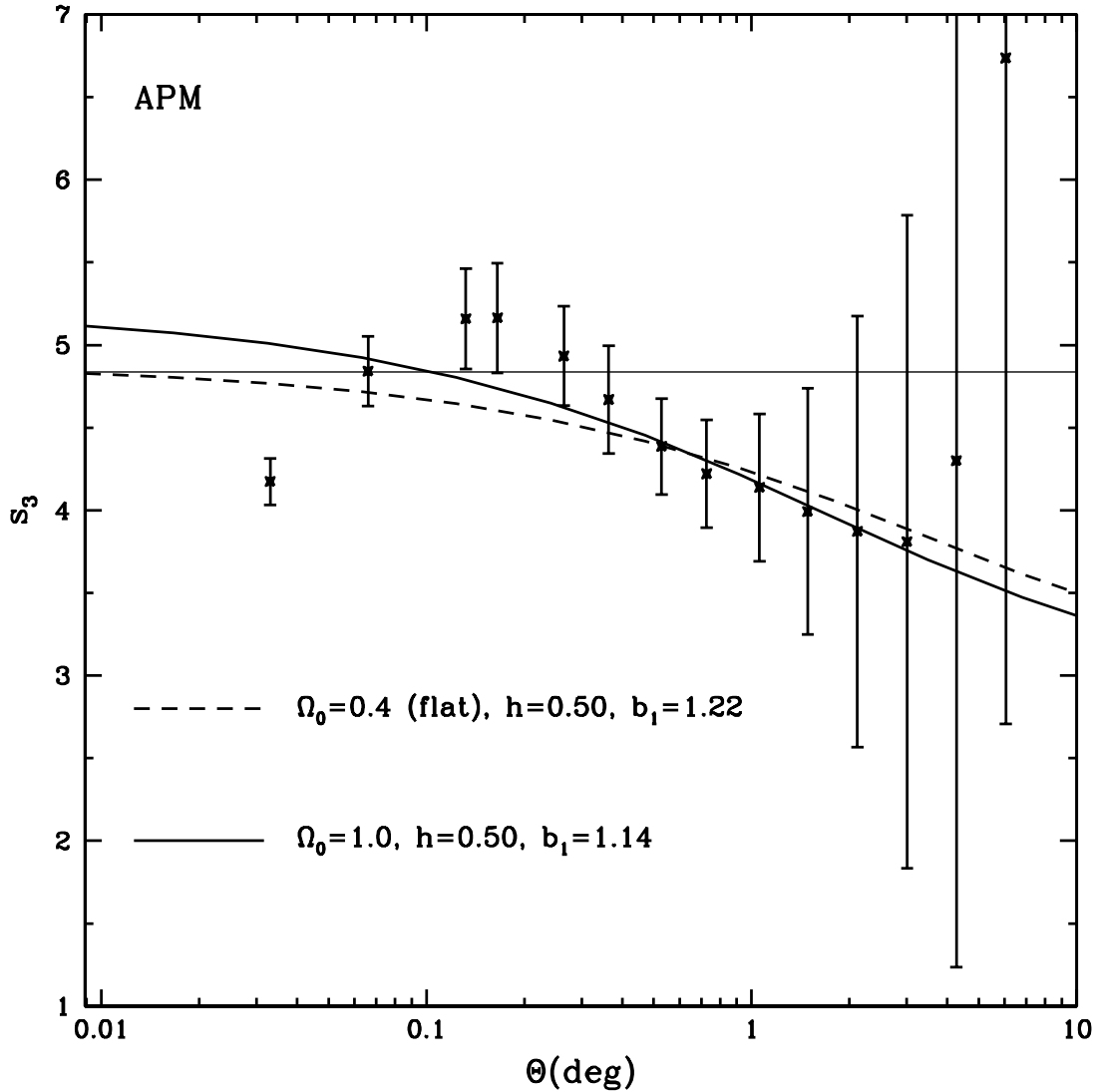


Fig. 7.— Comparison of APM-SF predictions for s_3 in the SCDM and Λ CDM models (with linear bias), with data from the APM Galaxy Survey (Gaztañaga 1994, 1997). While deviations are expected at small scales (from nonlinear and discreteness effects) and at large scales (from sample variance and the breakdown of the small-angle approximation), the data agree reasonably well, in the QL regime near 1° , with typical CDM models having a small amount of linear bias ($b_1 \sim 1.2 \pm 0.1$). The thin horizontal line is taken from Figure 3.

itself an unbiased estimator (Hui & Gaztañaga 1998), and 3) nonlinear effects not accounted for in our models (Boucher, Schaeffer, & Davis 1991; Jain & Bertschinger 1994; Scoccimarro *et al.* 1998; Scoccimarro & Frieman 1998; Munshi & Melott 1998). At large scales we expect discrepancies to arise from the breakdown of the small-angle approximation and the large scatter in the data induced by the smaller number of independently sampled cells. If we therefore exclude the data points at both the lower and upper ends of the range of Θ , and restrict the comparison to QL scales of $\Theta \lesssim 1^\circ$, where our predictions are expected to be valid, we find reasonable agreement with plausible CDM models having a small amount of linear bias. Of course, this conclusion is merely qualitative, as these data are clearly unable to place tight constraints on the models. The $2\text{-}\sigma$ error on b_1 in both models is roughly ± 0.1 , depending on exactly which points are excluded, in agreement with previous determinations of $b_1 \sim 1.0 \pm 0.2$ for the APM Survey (Baugh & Efstathiou 1993; Gaztañaga 1994; Bernardeau 1995). That the data for optically selected galaxies are roughly fit in the QL regime by the predicted values of s_3 in CDM models, requiring little or no bias (Gaztañaga 1994; Bernardeau 1995; Cappi & Maurogordato 1995; Roche & Eales 1998; Magliocchetti *et al.* 1998), lends some support to the scenario of gravitational evolution ensuing from Gaussian initial conditions, but better data are clearly needed. Note that the thin solid line, derived from equation (21) with the APM SF, no bias, and a constant power-law index of $n = -1.2$, yields a poorer fit in the QL range.

3. ANGULAR THREE-POINT CORRELATION FUNCTION

The normalized angular skewness, while containing some information about the overall dependence of clustering strength with scale, discards detailed and valuable information about the configuration dependence which is contained in the full angular 3PCF. It is known that the shape dependence of the spatial bispectrum and 3PCF, in leading order PT, can be used to distinguish between the effects of gravitational clustering and bias, as well as to obtain independent constraints on the linear- and nonlinear-bias parameters and on cosmological parameters (Jing & Zhang 1989; Fry 1994; Fry 1996; Jing & Börner 1997; Matarrese, Verde, & Heavens 1997; BK99). It stands to reason that the full angular 3PCF should also break these degeneracies and yield similar constraints. With this in mind, many authors have investigated the normalized angular 3PCF,

$$q(\theta_{12}, \theta_{23}, \theta_{31}) = \frac{Z(\theta_{12}, \theta_{23}, \theta_{31})}{\varpi(\theta_{12})\varpi(\theta_{23}) + \varpi(\theta_{12})\varpi(\theta_{31}) + \varpi(\theta_{23})\varpi(\theta_{31})}, \quad (32)$$

where the angular distances θ_{ij} form a triangle on the sky.

This quantity, which like s_3 is independent of the amplitude of the power spectrum,

was introduced based on empirical arguments for the so-called hierarchical model (Peebles 1975; Peebles & Groth 1975; Peebles 1980), and motivated by data which appeared to indicate that q was simply a constant. While equation (32) may be taken as a definition, the result for q in QL PT is, in general, *not* merely a constant; we demonstrate that the apparent constancy of q , as measured from past data, may simply be an artifact of coarse averaging over configuration shapes (Peebles & Groth 1975; Fry & Seldner 1982), combined with the effects of the shallow SFs which have characterized past surveys. There are, however, other problems associated with the definition of the normalized angular 3PCF in equation (32). In particular, q is apt to exhibit rapid variation and divergence where the denominator in equation (32) happens to acquire values of or near zero.⁷ This behavior is artificial in the sense that it does not reflect the true behavior of the 3PCF itself. BK99 demonstrate the analogous problems associated with the definition of the normalized spatial 3PCF, Q , and speculate that practical limitations in measuring this behavior may, in part, be responsible for observed discrepancies between QL PT predictions and those of N -body simulations. The skewness is less susceptible to this problem since it is scaled by the square of the variance, a positive-definite quantity. In places where q exhibits this rapidly-varying or divergent behavior, we will instead consider q_V , defined as $q_V = Z(\theta_{12}, \theta_{23}, \theta_{31})/(\sigma_{1^\circ})^4$, where $\sigma_{1^\circ} \equiv \sqrt{\varpi_{1^\circ}(0)}$ is the rms angular fluctuation on a smoothing scale of 1° , obtained for each model using equation (11). The chosen smoothing scale is, of course, arbitrary; we adopt a value of 1° as a convenient choice for the sake of graphical representation. Like q , q_V is independent of the overall normalization of the power spectrum, but it is not susceptible to the above mentioned problem associated with the definition of q . Observational measurements of both q and s_3 , however, will necessarily be ratios of estimators, and thus subject to associated errors discussed by Hui & Gaztañaga (1998).

Taking equation (4) with $x = \kappa\theta$ and omitting the window function, since we presume that the full CFs are now measured by direct counting, rather than by smoothed counts in cells, we obtain the direct-counting angular 2PCF,

$$\varpi(\theta) = \frac{A}{(2\pi)\theta^{n+2}} \int_0^{\eta_0} dw \frac{b_1^2 D^2(w)}{w^{n+2}} \left(\frac{dN}{dw} \right)^2 \int_0^\infty dx x^{n+1} T^2(x/\theta w) J_0(x). \quad (33)$$

The full angular 3PCF for projected triangles with sides of angular measures θ_{12} , θ_{23} , and

⁷We note that this problem is avoided entirely if one considers instead the normalized angular bispectrum in Fourier space.

θ_{31} can be evaluated using equation (12),

$$\begin{aligned}
Z(\theta_{12}, \theta_{23}, \theta_{31}) &= \frac{A^2}{(2\pi)^4} \int_0^{\eta_0} dw \frac{b_1^4 D^4(w)}{w^{2n+4}} \left(\frac{dN}{dw} \right)^3 \int_0^\infty d\kappa_1 \kappa_1^{n+1} T^2(\kappa_1/w) \\
&\times \int_0^\infty d\kappa_2 \kappa_2^{n+1} T^2(\kappa_2/w) \int_0^{2\pi} d\phi_1 \int_0^{2\pi} d\phi_2 e^{i(\boldsymbol{\kappa}_1 \cdot \boldsymbol{\theta}_{13} + \boldsymbol{\kappa}_2 \cdot \boldsymbol{\theta}_{23})} \\
&\times \left[\frac{1}{b_1} \left(1 + \mu + \cos \psi \left(\frac{\kappa_1}{\kappa_2} + \frac{\kappa_2}{\kappa_1} \right) + (1 - \mu) \cos^2 \psi \right) + \frac{b_2}{b_1^2} \right] \\
&\quad + (\text{cyc.}), \tag{34}
\end{aligned}$$

where ϕ_i is the angle between $\boldsymbol{\kappa}_i$ and $\boldsymbol{\theta}_{i3}$, ψ is the angle between $\boldsymbol{\kappa}_1$ and $\boldsymbol{\kappa}_2$, and similar conventions are used in each permutation term. Taking $x_i = \kappa_i \theta_{i3}$, and ϕ_{12} to be the angle between $\boldsymbol{\theta}_{13}$ and $\boldsymbol{\theta}_{23}$, so that

$$\cos \psi = \cos \phi_{12} (\cos \phi_1 \cos \phi_2 + \sin \phi_1 \sin \phi_2) + \sin \phi_{12} (\cos \phi_1 \sin \phi_2 - \sin \phi_1 \cos \phi_2), \tag{35}$$

and performing the ϕ_1 and ϕ_2 integrations, we have

$$\begin{aligned}
Z(\theta_{12}, \theta_{23}, \theta_{31}) &= \frac{A^2}{(2\pi)^2} \frac{1}{\theta_{31}^{n+2} \theta_{23}^{n+2}} \int_0^{\eta_0} dw \frac{b_1^4 D^4(w)}{w^{2n+4}} \left(\frac{dN}{dw} \right)^3 \int_0^\infty dx_1 x_1^{n+1} T^2(x_1/\theta_{31} w) \\
&\times \int_0^\infty dx_2 x_2^{n+1} T^2(x_2/\theta_{23} w) \left\{ \left(\frac{1 + \mu}{b_1} + \frac{b_2}{b_1^2} \right) J_0(x_1) J_0(x_2) \right. \\
&\quad - \frac{1}{b_1} \cos \phi_{12} \left(\frac{\theta_{23} x_1}{\theta_{13} x_2} J_1(x_1) J_1(x_2) + \frac{\theta_{13} x_2}{\theta_{23} x_1} J_1(x_1) J_1(x_2) \right) \\
&\quad + \frac{1 - \mu}{b_1} \left[\cos^2 \phi_{12} J_2(x_1) J_2(x_2) + \frac{1}{2} \mathcal{W}(x_1) \mathcal{W}(x_2) \right. \\
&\quad \left. \left. - \frac{1}{2} J_2(x_1) \mathcal{W}(x_2) - \frac{1}{2} J_2(x_2) \mathcal{W}(x_1) \right] \right\} + (\text{cyc.}). \tag{36}
\end{aligned}$$

For evolving bias we simply substitute

$$\left(\frac{1 + \mu}{b_1} + \frac{b_2}{b_1^2} \right) \longrightarrow C_1(w), \quad \frac{1}{b_1} \longrightarrow C_2(w), \quad \frac{1 - \mu}{b_1} \longrightarrow C_3(w) \tag{37}$$

inside the brackets, and replace b_1 by $1/C_2(w)$.

Equation (36) does not contain terms analogous to the higher-order terms in the sum in equation (20) [which gave rise to the $\Delta(n)$ term in equation (21)], since evaluation of the 3PCF by direct counting requires no smoothing. Using our model for unsmoothed bias, such terms *would* be induced in the calculation of the 3PCF using counts in cells, arising from factors of the form $\mathcal{W}(x\Theta/\theta)$ in the appropriate integrands. One must be careful to

realize that if the unsmoothed-bias prescription is correct, the nonlinear-bias parameter measured from the direct-counting angular 3PCF in equation (36) will be different from the smoothed value which could be inferred from s_3 or from the counts-in-cells 3PCF, though the two can be related, e.g., via the $\Delta(n)$ term in equation (21).

3.1. Effects of the Power Spectrum

For a scale-free power spectrum, equation (33) yields the familiar result, $\varpi(\theta) \propto \theta^{-(n+2)}$. For realistic CDM power spectra, there is a further dependence on θ which arises from the scale-dependence of the transfer function. Likewise, had we ignored the shape-dependent terms in the bispectrum in equation (15), we would find for power-law spectra the hierarchical approximation $Z(\theta_{12}, \theta_{23}, \theta_{31}) \propto \varpi(\theta_{12})\varpi(\theta_{23}) + \varpi(\theta_{12})\varpi(\theta_{31}) + \varpi(\theta_{23})\varpi(\theta_{31})$. These terms, however, introduce into equation (36) an additional, non-trivial dependence on the shape of the triangular configuration, even for the case of scale-free power spectra. Realistic models must account for this variation, as well as the scale dependence induced by the transfer function.

In order to interpret the results of the various CDM models, it will be instructive to first investigate the results obtained for Z for scale-free power spectra. In this case, we have

$$Z(\theta_{12}, \theta_{23}, \theta_{31}) = R_3(n) \left[\frac{10}{7} - \frac{\beta}{2-\beta} \cos \phi_{12} \left(\frac{\theta_{13}}{\theta_{23}} + \frac{\theta_{23}}{\theta_{13}} \right) + \frac{4}{7} \frac{(2-2\beta + \beta^2 \cos^2 \phi_{12})}{(2-\beta)^2} \right] \varpi(\theta_{13})\varpi(\theta_{23}) + (\text{cyc.}), \quad (38)$$

where $\varpi(\theta) \propto \theta^{-\beta}$ and $\beta = n + 2$. Figure 8 displays the results for $q/R_3(n)$ for $n = \{-1, -1.5, -2\}$ [recall $R_3(n)$ is of order unity, equal to $\{1.26, 1.19, 1.15\}$ and $\{1.21, 1.18, 1.17\}$ for these values of n , for the APM and high- z SFs, respectively]. Since q in this case is independent of overall scale, we specify the triangle configuration by fixing θ_{13} to have length 1, θ_{23} to have a relative length $u > 1$, and examine the variation of q with ϕ_{12} , for $u = 1, 3$, and the “limit” of $u \rightarrow \infty$. The Figure reveals shape dependence on both u and ϕ , the extent of which can (particularly in the case of the ϕ dependence) depend strongly on the index n . Specifically, we note that the amplitude of the shape variation tends to increase with increasing n . An “average” value for q can be obtained by taking $\langle \cos \phi \rangle = 0$ and $\langle \cos^2 \phi \rangle = 1/2$ in equation (38), yielding $\bar{q} = \frac{12}{7} R_3(n)$; while this is not generally valid, since the three angles appearing in the cyclic terms cannot be varied independently, this result is exactly true for all configurations when $\beta = 0$ (the no-smoothing case), as demonstrated by the thin, solid, horizontal line.

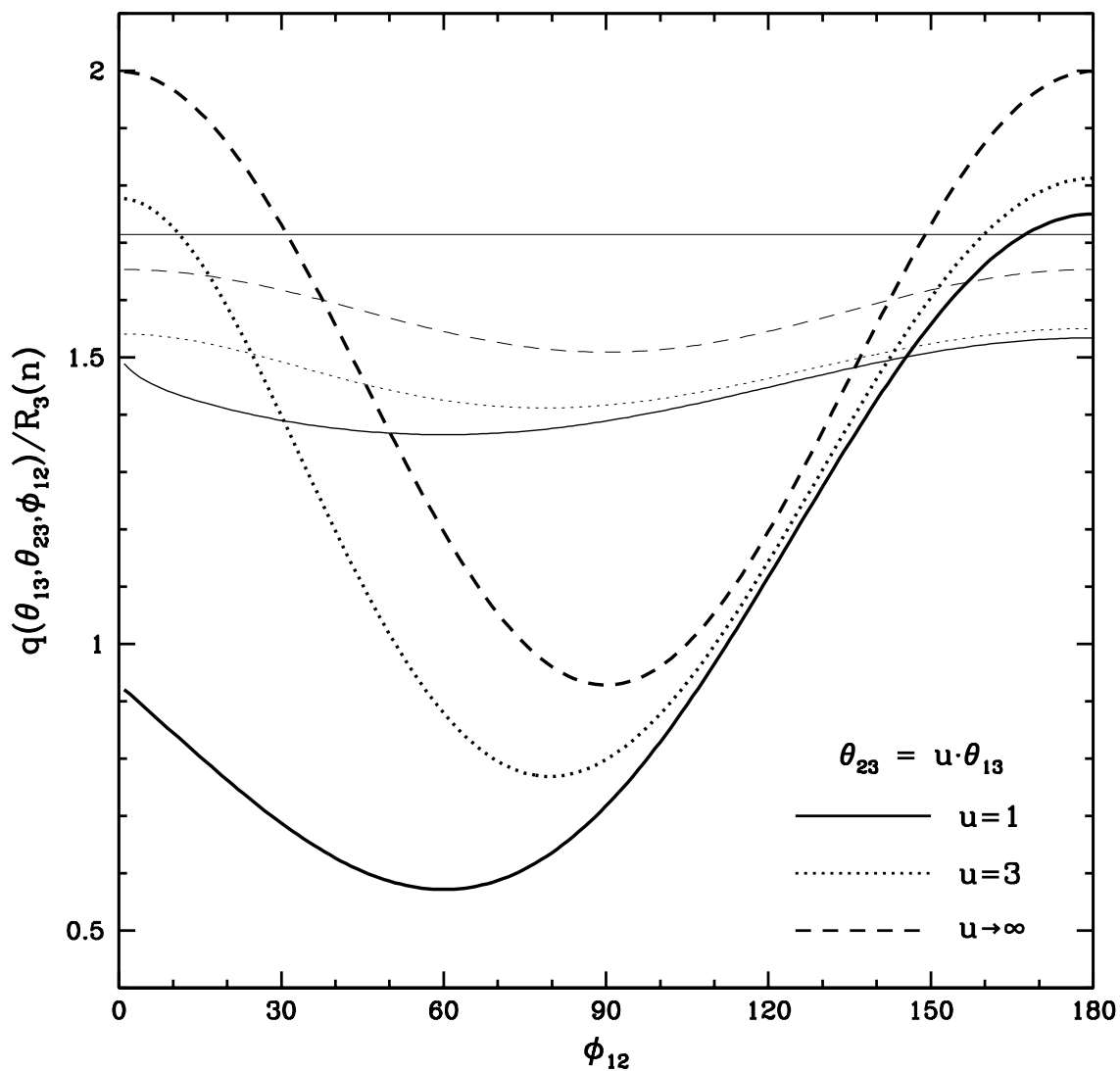


Fig. 8.— Results for $q(\theta_{13}, \theta_{23}, \phi_{12})/R_3(n)$ for power-law spectra with indices of $n = -1$, (thick lines), -1.5 (thin lines), and -2 (thin horizontal line). Since these results are independent of overall scale, we have fixed θ_{13} to have length 1, and vary θ_{23} in the manner shown. Note that the dependence of q on triangle shape varies strongly with n .

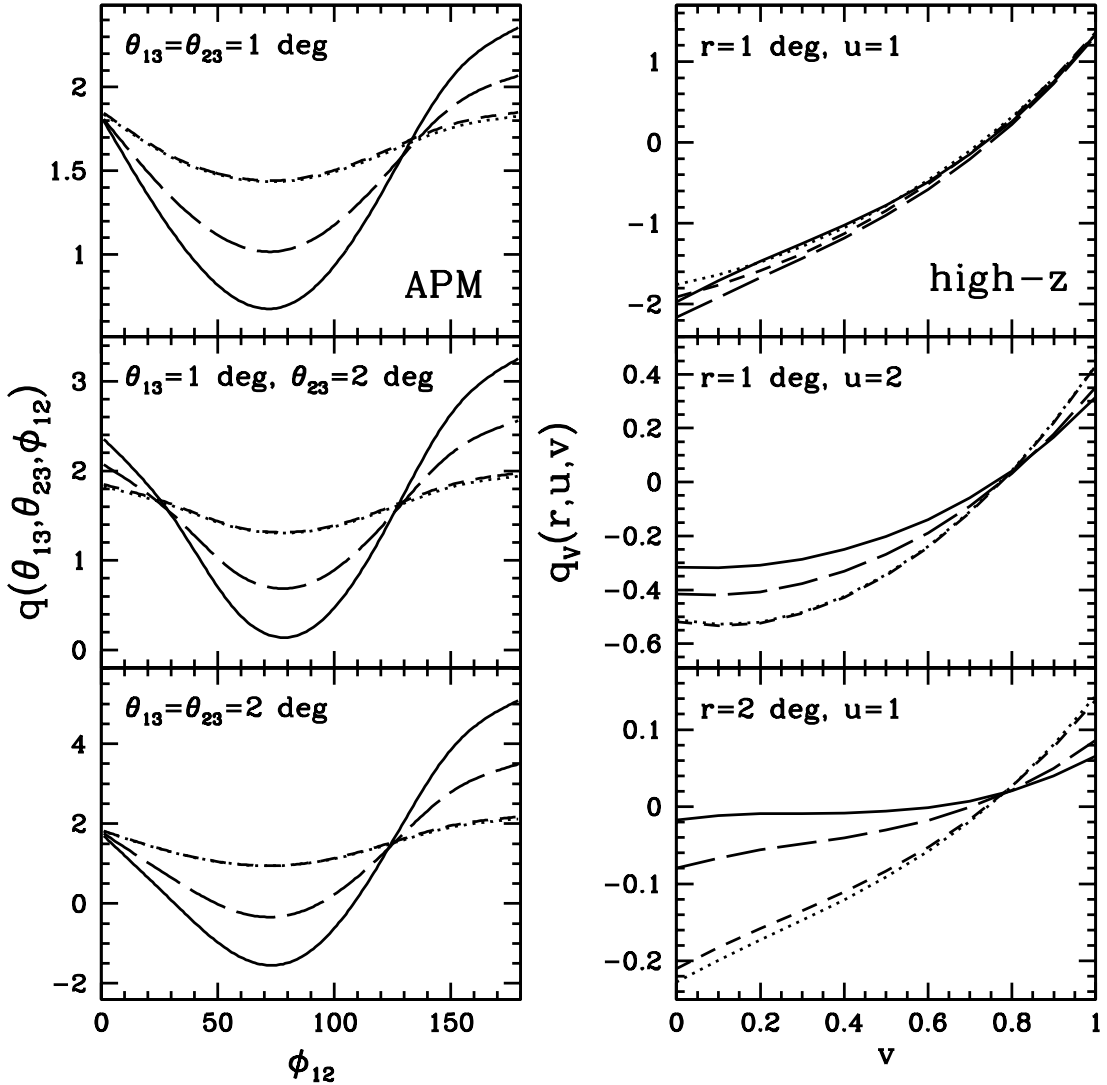


Fig. 9.— The left panels show results for q , assuming the APM SF, using the $\{\theta_{13}, \theta_{23}, \phi_{12}\}$ parameter set to define triangles. The right panels show the results for q_V for the same choice of configurations (assuming $\phi_{12} > 60^\circ$) using the $\{r, u, v\}$ parameter set. In both cases, the unbiased SCDM (solid lines), TCDM (long-dashed lines), Λ CDM (short-dashed lines), and OCDM (dotted lines) models are shown. Note that for both SFs, models with different values of Γ yield distinct predictions, and that the precise configuration dependence of the normalized 3PCF in each different model can vary appreciably with the SF.

In the left panels of Figure 9 we illustrate, for the APM SF, the behavior of $q(\theta_{13}, \theta_{23}, \phi_{12})$ for several configurations falling in the quasilinear regime, for an unbiased tracer mass in the SCDM, TCDM, Λ CDM and OCDM models. In this case, the results for the latter two models differ only by about the thickness of the curves, and can barely be distinguished. Other models, however, yield quite distinct predictions and might be differentiated on the basis of angular 3PCF measurements from large surveys. In particular, the SCDM and TCDM can be clearly distinguished from each other (BKJ show that this is not the case when considering the spatial 3PCF at $z = 0$), and from the low- Γ models, which show comparatively little variation with ϕ_{12} . Generally, we now find a dependence of q on scale (compare, e.g., the top and bottom panels) arising from the shape of the CDM transfer function. The observed shape dependence on θ_{23} (compare, e.g, the top and middle panels) and ϕ_{12} of these models can be understood in terms of the results for scale-free power spectra: over the scales considered here, the SCDM model has the largest effective power-spectrum index, while the low- Γ models have the smallest. The results for the APM SF shown in Figure 9 roughly agree with the predictions and N -body results of Frieman and Gaztañaga (1999). We thank them for pointing out an error in an earlier calculation of ours.

For a shallow SF such as that describing the APM Galaxy Survey, three points describing an elongated triangle in projection are more likely to correspond to a configuration which is elongated in real space. Thus, our results for q using the APM SF are similar to corresponding results for the normalized spatial 3PCF, Q (Fry 1984; Jing & Börner 1997), which predict that clustering in the mildly nonlinear regime favors elongated structures. For low- Γ models, however, the APM SF happens to yield predictions which do not vary strongly with either the shape or size of the triangular configuration. Since it is known that measurements of the power spectrum from surveys such as the APM favor models with low values of Γ (Efstathiou, Sutherland, & Maddox 1990; Baugh & Efstathiou 1993), it is not surprising that measurements of the angular 3PCF in shallow surveys have indicated it to be configuration independent, particularly given the present observational errors (Peebles and Groth 1975; Groth & Peebles 1977; Jing & Zhang 1989; Tóth, Hollósi, & Szalay 1989; Jing, Mo, & Börner 1991; Borgani, Jing, & Plionis 1991; Jing, & Börner 1998). While this has no doubt has lent support to the empirically-motivated hierarchical model which assumes Z to be, in fact, shape independent (i.e., $q = \text{constant}$), we demonstrate that the angular 3PCF, in general, can depend more significantly on the configuration and analysis of deeper angular surveys must take this variation into account.

The results for high- z SF for the same configurations (assuming $\phi_{12} > 60^\circ$ are shown in the right panels of Figure 9. We now plot q_V , since for this choice of SF the combination of 2PCFs appearing in the denominator of q can acquire values of or near zero in our models.

Furthermore, we now take the defining parameters for triangles projected on the sky to be

$$r = \theta_{12}, \quad u = \frac{\theta_{23}}{\theta_{12}}, \quad v = \frac{\theta_{31} - \theta_{23}}{\theta_{12}}, \quad (39)$$

where $\theta_{12} < \theta_{23} < \theta_{31}$, so that $u \geq 1$ and $0 \leq v \leq 1$ (Peebles & Groth 1975). For this choice of parameters, r effectively fixes the overall size of the triangle, while u and v determine the exact size and shape. Figure 6 in BK99 provides a graphical illustration of the variation of triangle geometry with r , u , and v . This parameterization is convenient since each choice of $\{r, u, v\}$ involves a minimum scale set by r . The $\{\theta_{13}, \theta_{23}, \phi_{12}\}$ parameter set, with $\theta_{13} = r$ and $\theta_{23} = ur$ is equivalent for ϕ_{12} ranging down to 60° , but for ϕ less than 60° this parameter set can sample scales (given by θ_{12}) all the way down to zero. Since we have chosen to normalize Z by the square of the variance at a fixed angular scale, the $\{\theta_{13}, \theta_{23}, \phi_{12}\}$ set can yield dramatically different amplitudes for q_V if $0^\circ < \phi_{12} < 60^\circ$ as opposed to those for $60^\circ < \phi_{12} < 180^\circ$, and is therefore less tenable.

Even once their different normalizations have been accounted for, we find that the high- z curves have significantly lower amplitudes than their APM-SF counterparts in the left panels. This is simply because projected triangles in a deeper survey can correspond to much larger physical triangles, for which the clustering amplitude will be significantly smaller. Since q_V is normalized by the square of the variance at a fixed scale, these plots now reveal clearly the expected decrease in clustering strength with increasing scale; this behavior, however, is not described simply by the $Z \propto \theta^{-2n+4}$ prediction of the hierarchical model. Unlike the APM case, we now find that *all* models show a significant variation with shape, as well as scale, with the low- Γ models in some cases now showing the strongest shape dependence. The SCDM and TCDM models appear less differentiated than in the APM case, but we find that the Λ CDM and OCDM models can now differ somewhat more substantially, particularly on larger scales, since deeper surveys are more sensitive to cosmological effects. Most importantly, however, we still find overall that the high- Γ and low- Γ models can be fairly well resolved on 2° scales, and the distinction increases for larger scales. Naturally, a thorough comparison with measurements spanning the full configuration space in a more complete fashion would allow for better discrimination among models.

3.2. Effects of Bias and its Evolution

The results for the different bias scenarios investigated in §2.2 are demonstrated in Figure 10, which shows q_V , assuming $r = 1^\circ$ and $u = 1$, for the Λ CDM (thick lines) and OCDM (thin lines) models, for the high- z SF. Though this is only one slice of the parameter

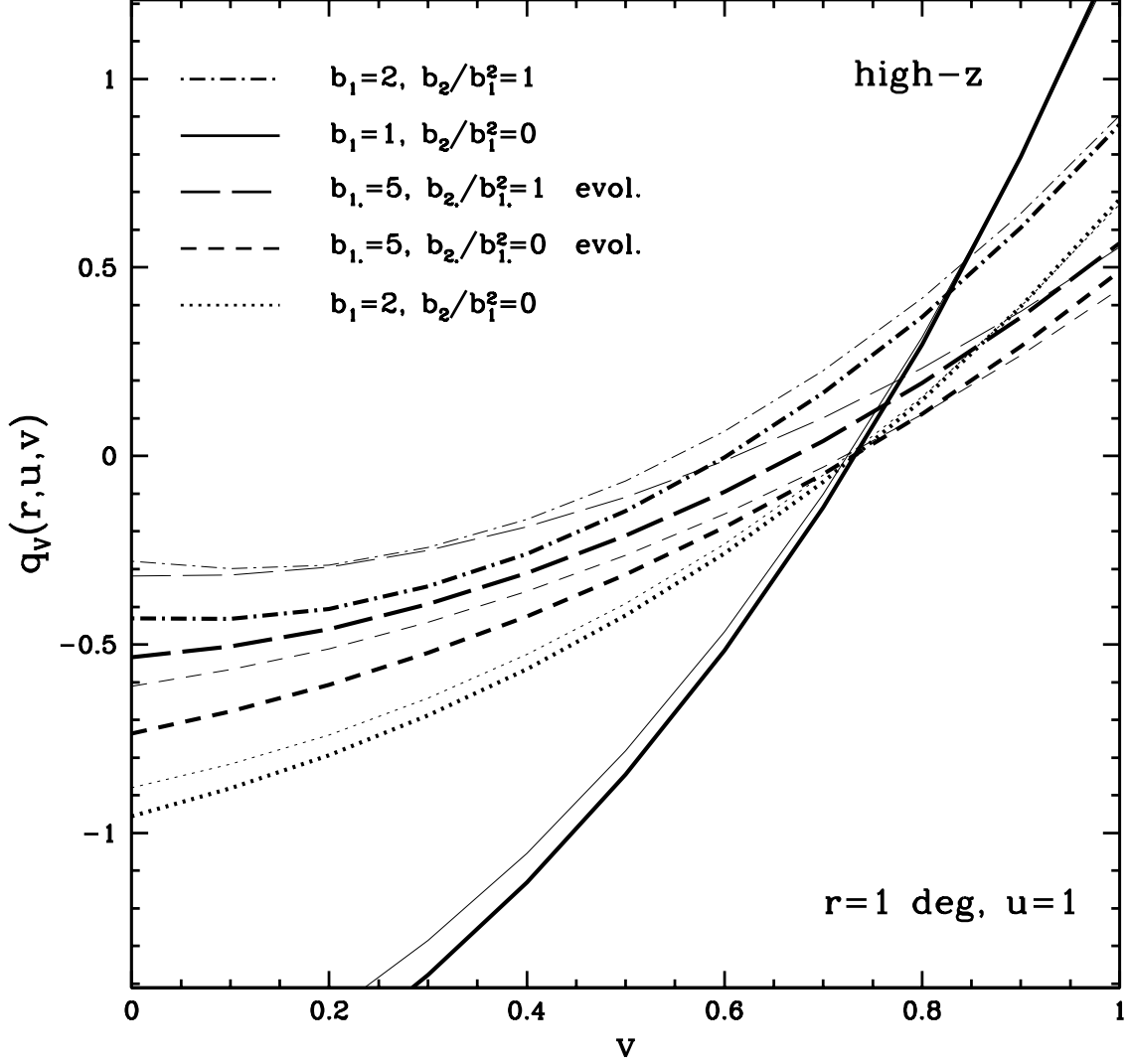


Fig. 10.— Plot of $q_V(v)$, assuming fixed $r = 1^\circ$ and $u = 1$, for the five bias scenarios from §2.2, each employing the Λ CDM (thick lines) and OCDM (thin lines) models, and using the high- z SF. Note the respectively similar influences of the biasing models as were seen with s_3 (Figures 5 and 6).

space we are exploring, we use it to illustrate the similar dependences of the full angular 3PCF on the bias scheme as were seen for s_3 . In particular, we see a general flattening and reduction of q_V with increasing linear bias, and a relative increase with increasing nonlinear bias, as compared with the corresponding linear scheme. Note the slightly different predictions between these two models, arising from their different expansion histories; these differences would be greater for lower values of Ω_0 . As with s_3 (see Figures 5 and 6), it is clear that measurements of q_V should be able distinguish between the effects of a significant bias and those arising simply from unbiased gravitational evolution.

Consideration of the full configuration dependence of the angular 3PCF, however, allows for much better discrimination between different cosmological and biasing schemes than could be obtained from the skewness alone. It is known that measurements of the bispectrum and 3PCF can be used to obtain independent constraints on the constant-valued linear- and nonlinear-bias parameters (Fry & Gaztañaga 1993; Fry 1994, 1996; Jing 1997; Matarrese, Verde, & Heavens 1997, BK99). This can be inferred here from the different manners in which b_1 and b_2 appear in equation (36); the different weightings of these two parameters is sampled for every triangular configuration, producing a graph such as Figure 10 for every pair of values (r, u) [as opposed to s_3 , which yields only one constraint on the combination of $b_1(t)$ and $b_2(t)$]. As another example of the added information which can be gleaned from the full geometric dependence of the full 3PCF, we plot in Figure 11 $q_V(r, u, v)$, assuming the high- z SF, for two of our bias scenarios: the SCDM constant, linear-bias model (with $b_1 = 2$ and $b_2 = 0$), and the SCDM evolving linear-bias model (with $b_{1*} = 5$ and $b_{2*} = 0$). These two cases yielded nearly identical results for s_3 in Figure 6 (where evolving, linear bias effectively approximated a smaller, constant, linear bias), particularly on scales near 1° . Here, we see that by considering the variation of q_V with triangle geometry, the degeneracy between constant and evolving bias can be alleviated, to a degree, because the angular 3PCF probes a broad range of redshifts and allows us to see the effects of evolution in projection. BK99 show that these evolving and non-evolving bias models might also be distinguished using measurements of ζ as a function of redshift in a deep ($\bar{z} \gtrsim 1$) survey, or, to a lesser extent, by large-scale ($R \gtrsim 20$ Mpc) measurements of ζ at $z = 0$. In practice, however, measuring the angular 3PCF over scales of $\Theta \sim 1^\circ$ in a deep optical survey, or a radio survey such as the VLA FIRST Survey, may be more feasible and would likely yield stronger statistical constraints.

The parameter values we have investigated here are only intended as illustrations. The full statistical power which could be gained by exploring both the configuration and evolutionary dependences of Z in a complete fashion could be useful in distinguishing between the signatures of gravitational evolution versus bias, independently measuring the linear- and nonlinear-bias parameters, and constraining the shape of the power spectrum.

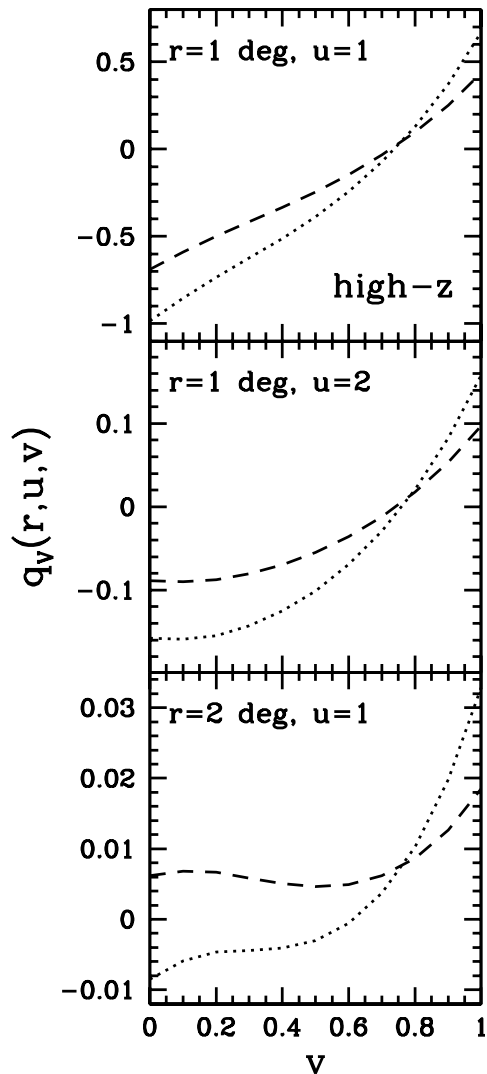


Fig. 11.— Plot of $q_V(r, u, v)$, assuming the high- z SF, for the SCDM model with constant, linear bias (dotted lines) and the SCDM model with evolving linear bias (short-dashed lines) from Figure 6. While these models yielded nearly degenerate predictions for s_3 in Figure 6, they are better distinguished here by virtue of the different configuration dependences of their full angular 3PCFs.

With better data, as might be obtained from emerging surveys, one could further determine the linear evolution of the power spectrum and of the bias, which in turn provide direct constraints on Ω_0 , Ω_Λ , and possibly the epoch of galaxy formation. However, it is already clear from Figures 9–11 that the behavior of the angular 3PCF is not simply that of the hierarchical model which assumes q to be a shape-independent constant, and further that, in addition to the full geometric dependence, one must consider the detailed dependences on the forms and evolutionary behaviors of the power spectrum, the biasing mechanism, and the selection function, as these can have a substantial impact on the results, particularly for high-redshift surveys.

4. CONCLUSION

We have calculated the leading-order results for the normalized angular skewness and 3PCF, assuming Gaussian initial conditions, for an arbitrary, biased tracer-mass distribution in flat and open universes. We have considered two selection functions, intended to represent low-redshift ($\bar{z} \sim 0.1$) and high-redshift ($\bar{z} \sim 1.0$) surveys. Our derivations incorporate such features as the scale dependence and linear evolution of the CDM power spectrum and the presence of a possibly evolving linear or nonlinear bias. Our results for s_3 for the case of an unbiased tracer mass are in agreement with previous work (Fry & Gaztañaga 1993; Bernardeau 1995) and we confirm that PT predictions for s_3 in typical CDM models, with a small amount of linear biasing ($b_1 \sim 1.15 \pm 0.1$), agree in the QL regime with data from the APM Galaxy Survey. Similar to BK99, we extend the result for s_3 in the case of nonlinear bias, to include a scale-dependent, leading-order correction which becomes significant for positive effective spectral indices, corresponding to scales $\Theta \gtrsim 5^\circ$ for CDM models. This correction term can be used to relate the unsmoothed nonlinear-bias parameter defined in the limit of continuous fields, with the traditionally-used, scale-dependent, nonlinear-bias parameter defined for smoothed density fields. For a given CDM model, this large-scale behavior of s_3 might alone allow a more accurate determination of the linear- and nonlinear-bias parameters (or at least discriminate between the smoothed and unsmoothed bias formulations), if other factors, such as sampling variance and the breakdown of the small-angle approximation, can be addressed.

We also derive predictions for the normalized angular 3PCF, considering q_V rather than q in cases where the latter is ill-behaved. We show that Z , as predicted by QL PT, is not given simply by the form of the “empirical” hierarchical model, i.e., with q simply a constant of order unity, but has a more complex dependence on scale, shape,

and expansion history. While for shallow SFs the weak shape dependence of q , combined with measurements coarsely averaged over configuration shapes, can yield results consistent with this hierarchical model, ignoring the detailed geometric and evolutionary variations of the angular 3PCF in general can destroy much valuable information. In several cases, we illustrate explicitly the importance of the various evolutionary dependences which factor into our calculations of angular statistics, such as the linear evolution of the power spectrum, the evolution of the bias parameters, and the Ω_0 dependence of the SFs. The proper treatment of these detailed dependences will be important in interpreting data from the emerging generation of deep, high-precision surveys, particularly when considering the high-redshift universe.

We find that biasing plays a major role in predictions for s_3 and Z . In particular, the scale dependence of s_3 and the configuration dependence of q (or q_V) bear characteristic imprints of bias, such as a relative flattening and decrease with increasing b_1 and a relative increase with increasing b_2 . Compared with the dependence on the biasing scenario, the dependence of s_3 on the cosmological model is fairly weak. This is not the case, however, for q , which can vary appreciably with the values of Γ and n . Though s_3 preserves information about the overall scale dependence of the 3PCF, it provides only one constraint on the combination of the cosmological parameters, $b_1(t)$, and $b_2(t)$, leaving various possible degeneracies between these quantities, including the degeneracy between constant- and evolving-bias models. These can be partially alleviated by considering the dependence of the normalized angular 3PCF on the projected-triangle geometry. In particular, the variation of q can be used to distinguish between the effects of gravitational evolution and bias, place constraints on the value of Γ and the shape of the power spectrum, measure the bias terms b_1 and b_2 and their time evolution, and perhaps constrain Ω_0 directly. Comparing predictions for s_3 and q with several data sets characterizing different tracer populations could allow multiple, complementary constraints on these important quantities.

While many of the results obtained here for s_3 and Z are qualitatively similar to the corresponding results obtained by BK99 for their spatial counterparts, S_3 and ζ , the use of angular statistics offers many practical advantages, such as greater statistical power and the absence of redshift distortions, which warrant their separate consideration. Our derivations have also relied on specific assumptions, such as the chosen bias-evolution model and the validity of both the small-angle approximation and the assumption of quasilinearity. Based on analogous results from three-dimensional calculations, we expect that qualitative features such as the upturn in s_3 at large smoothing angles in the case of nonlinear bias, the reduced configuration (scale) dependence of q (s_3) with increasing linear bias of any form, and the sensitivity of q to the shape of the power spectrum will be retained in more general calculations.

The utility of the predictions for s_3 and q will of course rely on the precision with which these statistics can be measured. While current data, of the type shown in Figure 7, is clearly insufficient to obtain strong constraints on the shape of the power spectrum or on the bias parameters, it is hoped that future surveys, such as the SDSS, will greatly improve upon this situation. In particular, if we optimistically assume the relevant uncertainties to be predominantly statistical, we can infer that the errors in measurements of s_3 from the SDSS will be roughly a factor of ten smaller than those in Figure 7. Of course, the comparison of predictions with two-dimensional survey data will require the additional consideration of systematic effects. Among these are finite-volume and boundary effects, which can have a significant impact on degree scales and above (Baugh, Gaztañaga, & Efstathiou 1995; Szapudi & Colombi 1996; Colombi, Szapudi, & Szalay 1998; Gaztañaga & Bernardeau 1998; Munshi & Melott 1998), estimation biases (Hui & Gaztañaga 1998; Kerscher 1998), Poisson noise (Peebles 1980; Gaztañaga 1994), and sampling variance (Seto & Yokoyama 1998). Gaztañaga & Bernardeau (1998) also find that QL PT predictions for angular statistics may underestimate projection effects, particularly for APM-type surveys.

In addition, the above calculations can be extended in several ways. For example, one might consider stochastic-biasing models which may yield different results, particularly on smaller scales (Fry & Gaztañaga 1993; Catelan *et al.* 1998; Catelan, Matarrese, & Porciani 1998; Taruya, Koyama & Soda 1998; Blanton *et al.* 1998; Colín *et al.* 1998; Taruya & Soda 1998; Narayanan, Berlind, & Weinberg 1998). Several authors have also investigated the impact of higher-order nonlinear terms in PT calculations (Jain & Bertschinger 1994; Scoccimarro & Frieman 1996a,b; Scoccimarro *et al.* 1998; Heavens, Matarrese, & Verde 1998; Scoccimarro & Frieman 1998), also expected to become important on smaller scales, where $\varpi \gtrsim 1$. Similar calculations can also be performed for higher-order angular moments and n -point CFs, such as the kurtosis and four-point correlation function, and so on (Suto & Matsubara 1994; Bernardeau 1994; Lokas *et al.* 1995; Gaztañaga & Bernardeau 1998), which, in principle, provide additional, independent constraints. The formalism can also be applied to structure-formation models with non-Gaussian initial conditions, such as topological-defect or isocurvature models, to investigate how these might be distinguished from inflationary models (Luo & Schramm 1993; Jaffe 1994; Fry & Scherrer 1994; Chodorowski & Bouchet 1996; White 1998).

We are indebted to J. Frieman and E. Gaztañaga for helpful discussions and suggestions, and in particular for their help in clarifying an earlier problem in the calculation. We also wish to thank R. Scoccimarro, as well as Licia Verde, for numerous helpful comments and discussions. This work was supported at Columbia by D.O.E. contract DEFG02-92-ER 40699, NASA NAG5-3091, NSF AST94-19906, and the Alfred P. Sloan Foundation, and at

Berkeley by NAG5-6552.

A. PROJECTED BISPECTRUM

In this Appendix, we derive a simple Fourier-space analogue of Limber’s equation for the bispectrum of the two-dimensional projection of a three-dimensional scalar field. Our derivation is similar to that of Kaiser (1992), who calculated the projected (two-point) power spectrum. We first consider the case of an Einstein-de Sitter universe and at the end we generalize the results to open or closed universes. Jaffe & Kamionkowski (1998) discuss a different application of this formalism to isotropic vector fields.

Consider a three-dimensional field, $\delta(\mathbf{x}, w)$, at a conformal lookback time w , and its Fourier transform, $\tilde{\delta}(\mathbf{k}, w)$. We will take δ to have zero mean (or subtract the mean explicitly). To project onto the two-dimensional sky, we apply the “selection function,” $q(w)$, and denote the resulting field by

$$p(\boldsymbol{\theta}) = \int_0^\infty dw q(w) \delta(w\boldsymbol{\theta}_1, w\boldsymbol{\theta}_2, w, w), \quad (\text{A1})$$

where $\boldsymbol{\theta}$ is a two-dimensional vector on the sky pointed at by the three-dimensional unit vector $\hat{\boldsymbol{\theta}}$. We consider only small patches, and thus can perform a two-dimensional Fourier transform on essentially flat areas of sky, giving $\tilde{p}(\boldsymbol{\kappa})$, where $\boldsymbol{\kappa}$ denotes two-dimensional Fourier-space vectors. As in Kaiser (1992), the contribution from a thin shell of width Δw centered at w_0 to $\tilde{p}(\boldsymbol{\kappa})$ is

$$\widetilde{\Delta p}(\boldsymbol{\kappa}) = \frac{\Delta w q(w_0)}{w_0^2} \int \frac{dk_3}{2\pi} \tilde{\delta}\left(\frac{\kappa_1}{w_0}, \frac{\kappa_2}{w_0}, k_3, w\right) j_0\left(\frac{k_3 \Delta w}{2}\right), \quad (\text{A2})$$

where the $j_0(x) = \sin x/x$ factor arises from the integral of $\exp(-i\mathbf{k}_3 \cdot \mathbf{w})$ over the shell.

We define the three-dimensional bispectrum, the Fourier-space analogue of the three-point function, by

$$\langle \tilde{\delta}(\mathbf{k}) \tilde{\delta}(\mathbf{k}') \tilde{\delta}(\mathbf{k}'') \rangle = (2\pi)^3 \delta_D(\mathbf{k} + \mathbf{k}' + \mathbf{k}'') B(\mathbf{k}, \mathbf{k}', \mathbf{k}''); \quad (\text{A3})$$

the two-dimensional analogue is

$$\langle \tilde{p}(\boldsymbol{\kappa}) \tilde{p}(\boldsymbol{\kappa}') \tilde{p}(\boldsymbol{\kappa}'') \rangle = (2\pi)^2 \delta_D(\boldsymbol{\kappa} + \boldsymbol{\kappa}' + \boldsymbol{\kappa}'') B_p(\boldsymbol{\kappa}, \boldsymbol{\kappa}', \boldsymbol{\kappa}''), \quad (\text{A4})$$

where the dimensionality of the Dirac delta function is obvious from its arguments.

We can form the contribution to the two-dimensional bispectrum from the thin shell,

$$\begin{aligned} \langle \widetilde{\Delta p}(\boldsymbol{\kappa}) \widetilde{\Delta p}(\boldsymbol{\kappa}') \widetilde{\Delta p}(\boldsymbol{\kappa}'') \rangle &= (2\pi)^2 \delta_D(\boldsymbol{\kappa} + \boldsymbol{\kappa}' + \boldsymbol{\kappa}'') \frac{[q(w_0)\Delta w]^3}{w_0^4} \int \frac{dk_3}{2\pi} \frac{dk'_3}{2\pi} \\ &\times j_0\left(\frac{k_3\Delta w}{2}\right) j_0\left(\frac{k'_3\Delta w}{2}\right) j_0\left(\frac{k''_3\Delta w}{2}\right) B(r, r', r''), \end{aligned} \quad (\text{A5})$$

where

$$r = \sqrt{\frac{\kappa_1^2 + \kappa_2^2}{w_0^2} + k_3^2}. \quad (\text{A6})$$

Now, we make the same simplifying assumptions as in the original Kaiser derivation: the shells have width $\Delta w/w \ll 1$ but are thick compared to wavelengths contributing to δ of interest, so $\Delta w/w \gg 1/\kappa$. Since the j_0 factors have width $\Delta k_3 \sim 1/\Delta w$, we can pull the B out of the integral and set $r = r|_{k_3=0} = \kappa/w_0$; only modes perpendicular to the line of sight contribute in the small-angle approximation. Then using the identity,

$$\int_{-\infty}^{\infty} \int_{-\infty}^{\infty} j_0(x) j_0(y) j_0(x+y) dx dy = \pi^2, \quad (\text{A7})$$

we can write the contribution from the shell as

$$\langle \widetilde{\Delta p}(\boldsymbol{\kappa}) \widetilde{\Delta p}(\boldsymbol{\kappa}') \widetilde{\Delta p}(\boldsymbol{\kappa}'') \rangle = (2\pi)^2 \delta_D(\boldsymbol{\kappa} + \boldsymbol{\kappa}' + \boldsymbol{\kappa}'') \frac{q(w_0)^3 \Delta w}{w_0^4} B\left(\frac{\kappa}{w}, \frac{\kappa'}{w}, \frac{\kappa''}{w}\right). \quad (\text{A8})$$

The bispectrum is a ‘‘cumulant’’; that is, contributions to the total bispectrum simply add. Thus, we can sum up the contributions from different shells, and convert the sum to an integral:

$$\langle \widetilde{p}(\boldsymbol{\kappa}) \widetilde{p}(\boldsymbol{\kappa}') \widetilde{p}(\boldsymbol{\kappa}'') \rangle = (2\pi)^2 \delta(\boldsymbol{\kappa} + \boldsymbol{\kappa}' + \boldsymbol{\kappa}'') \int dw \frac{q(w)^3}{w^4} B\left(\frac{\kappa}{w}, \frac{\kappa'}{w}, \frac{\kappa''}{w}; w\right); \quad (\text{A9})$$

with the full definition of the bispectrum, this just gives the desired formula,

$$B_p(\boldsymbol{\kappa}, \boldsymbol{\kappa}', \boldsymbol{\kappa}'') = \int dw \frac{q(w)^3}{w^4} B\left(\frac{\kappa}{w}, \frac{\kappa'}{w}, \frac{\kappa''}{w}; w\right) \quad (\text{A10})$$

(allowing the three-dimensional bispectrum to vary with lookback time, w). Note that the integrand in the formula is weighted by q^3/w^4 ; this is in contrast to the (two-point) power spectrum version of the calculation which weights by q^2/w^2 [see equation (6)]. Hence, the bispectrum is weighted considerably more heavily to late times (small w).

To generalize to an open or closed Universe, we must replace the distances w in the derivation above with the angular-diameter distance. Thus in an open or closed Universe one replaces

$$\frac{1}{w} \longrightarrow \frac{a_0 H_0 \sqrt{|1 - \Omega_0 - \Omega_\Lambda|}}{S(a_0 H_0 w \sqrt{|1 - \Omega_0 - \Omega_\Lambda|})} \quad (\text{A11})$$

in the first three arguments of $B(\kappa/w, \kappa'/w, \kappa''/w; w)$ and in the w^4 in the denominator in equation (A10), where $S(x) = \sinh x$ in an open Universe and $S(x) = \sin x$ in a closed Universe.

REFERENCES

- Baugh, C. M. *et al.* 1998, astro-ph/9811222, MNRAS, submitted
- Baugh, C. M. & Efstathiou, G. 1993, MNRAS, 265, 145
- Baugh, C. M., Gaztañaga, E., Efstathiou, G. 1995, MNRAS, 274, 1049
- Bardeen, J. M. *et al.* 1986, ApJ, 304, 15
- Bartlett, J. G. *et al.* 1998, Fundamental Parameters in Cosmology, Les Arcs; Publisher: Editions Frontieres, p. 103
- Becker, R. H., White, R. L., & Helfand, D. J. 1995, ApJ, 450, 559
- Bernardeau, F. 1994, ApJ, 433, 1
- Bernardeau, F. 1995, A&A, 301, 309
- Blanton, M. *et al.* 1998, astro-ph/9807029, ApJ, submitted
- Borgani, S., Jing, Y., & Plionis, M. 1992, ApJ, 395, 339
- Bouchet, F. R. *et al.* 1992, ApJ, 394, L5
- Bouchet, F. R. *et al.* 1995, A&A, 296, 575
- Bouchet, F. R. & Hernquist, L. 1992, ApJ, 400, 25
- Bouchet, F. R., Schaeffer, R., & Davis, M. 1991, ApJ, 383, 19
- Buchalter, A. & Kamionkowski, M. 1999, ApJ, 521, in press
- Cappi, A. & Maurogordato, S. 1995, ApJ, 438, 507
- Catelan, P. *et al.* 1995, MNRAS, 276, 39
- Catelan, P. *et al.* 1998, MNRAS, 297, 692
- Catelan, P., Matarrese, P., & Porciani, C. 1998, ApJ, 502, L1
- Chodorowski, M. J. & Bouchet, F. R. 1996, MNRAS, 279, 557
- Colín, P. *et al.* 1998, astro-ph/9809202, ApJ, submitted
- Colombi, S., Szapudi, I., & Szalay, A. 1998, MNRAS, 296, 253
- Cress, C. M. *et al.* 1996, ApJ, 473, 7
- Cress, C. M. & Kamionkowski, M. 1998, MNRAS, 297, 486
- Efstathiou, G., Sutherland, W. J., & Maddox, S. J. 1990, Nat, 348, 705
- Frieman, J. A. & Gaztañaga, E. 1999, in preparation
- Frieman, J. A. & Gaztañaga, E. 1994, ApJ, 425, 392

- Fry, J. N. 1984, ApJ, 279, 499
- Fry, J. N. 1994, PRL, 73, 215
- Fry, J. N. 1996, ApJ, 461, L65
- Fry, J. N. & Gaztañaga, E. 1993, ApJ, 413, 447
- Fry, J. N., Melott, A. L., & Shandarin, S. F. 1993, ApJ, 412, 504
- Fry, J. N., Melott, A. L., & Shandarin, S. F. 1995, MNRAS, 274, 745
- Fry, J. N. & Scherrer, R. J. 1994, ApJ, 429, 36
- Fry, J. N. & Seldner, M. 1982, ApJ, 259, 474
- Gaztañaga, E. 1994, MNRAS, 268, 913
- Gaztañaga, E. 1997, private communication
- Gaztañaga, E. & Baugh, C. M. 1998, MNRAS, 294, 229
- Gaztañaga, E. & Bernardeau, F. 1998, A&A, 331, 829
- Gaztañaga, E., Croft, R. A. C., & Dalton, G. B. 1995, MNRAS, 276, 336
- Gaztañaga, E. & Frieman, J. A. 1994, ApJ, 437, L13
- Goroff, M. H. *et al.* 1986, ApJ, 311, 6
- Gott, J. R., Gao, B. & Park, C 1991, ApJ, 383, 90
- Gradshteyn, I. S. & Ryzhik, I. M. 1980, Table of Integrals, Series, and Products, Academic Press, New York
- Groth, E. J. & Peebles, P. J. E. 1977, ApJ, 217, 385
- Heavens, A. F., Matarrese, S., & Verde, L. 1998, astro-ph/9808016, MNRAS, in press
- Hui, L. & Gaztañaga, E. 1998, astro-ph/9810194, ApJ, submitted
- Jaffe, A. H. 1994, Phys. Rev. D, 49, 3893
- Jaffe, A. H. & Kamionkowski, M. 1998, Phys. Rev. D58 043001
- Jain, B. & Bertschinger, E. 1994, ApJ, 431, 495
- Jensen, L. G. & Szalay, A. S. 1986, 305, L5
- Jing, Y. 1997, Proceedings of IAU Symposium 183, Cosmological parameters and the evolution of the Universe, August 18-22, Kyoto
- Jing, Y. & Börner, G. 1997, A&A, 318, 667
- Jing, Y. & Börner, G. 1998, ApJ, 503, 37
- Jing, Y., Mo, H. J. & Börner, G. 1991, A&A, 252, 449

- Jing, Y. & Zhang, J. 1989, ApJ, 342, 639
- Juszkiewicz, R., Bouchet, F.R., & Colombi S. 1993, ApJ, 412, L9
- Kaiser, N. 1992, ApJ, 388, 272
- Kamionkowski, M. & Buchalter, A. 1998, ApJ, in press
- Kerscher, M. 1998, astro-ph/9811300, A&A, accepted
- Lokas, E. L. *et al.* 1995, MNRAS, 274, 730
- Loveday, J. *et al.* 1998, Wide Field Surveys in Cosmology, Paris; Publisher: Editions Frontieres, p. 317
- Luo, X. & Schramm, D. N. 1993, ApJ, 408, L33
- Maddox, S. J., Efstathiou, G., & Sutherland, W. J. 1996, MNRAS, 283, 1227
- Magliocchetti, M. *et al.* 1998, MNRAS, 300, 257
- Magliocchetti, M. & Maddox, S. J. 1998, astro-ph/9811320, MNRAS, submitted
- Martel, H. 1995, ApJ, 445, 537
- Matarrese, S., Verde, L., & Heavens, A. F. 1997, MNRAS, 290, 651
- Matarrese, S. *et al.* 1997, MNRAS, 286, 115
- Mo, H. J. & White, S. D. M. 1996, MNRAS, 282,347
- Munshi, D. & Melott, A. L. 1998, astro-ph/9801011
- Narayanan, V. K., Berlind, A. A., & Weinberg, D. H. 1998, astro-ph/9812002, ApJ, submitted
- Peacock, J. A. 1997, MNRAS, 284, 885
- Peebles, P. J. E. 1975, ApJ, 196, 647
- Peebles, P. J. E. 1980, The Large-Scale Structure of the Universe, Princeton University Press, Princeton
- Peebles, P. J. E. & Groth, E. J. 1975, ApJ, 196, 1
- Roche, N & Eales, S. A. 1998, MNRAS, submitted
- Scoccimarro, R. 1998, private communication
- Scoccimarro, R. *et al.* 1998, ApJ, 496, 586
- Scoccimarro, R., Couchman, H. M. P., & Frieman, J. A. 1998, astro-ph/9808305, ApJ, accepted
- Scoccimarro, R. & Frieman, J. A. 1996a, ApJ Supp., 105, 37

- Scoccimarro, R. & Frieman, J. A. 1996b, *ApJ*, 473, 620
- Scoccimarro, R. & Frieman, J. A. 1998, astro-ph/9811184, *ApJ*, accepted
- Seto, N. & Yokoyama, J. 1998, astro-ph/9812221
- Steidel, C. *et al.* 1998, *ApJ*, 492, 428
- Suto, Y. & Matsubara, T. 1994, *ApJ*, 420, 504
- Szalay, A. S. 1988, *ApJ*, 333, 21
- Szapudi, I. & Colombi, S. 1996, *ApJ*, 470, 131
- Szapudi, I. *et al.* 1988, astro-ph/9810190, *ApJ*, submitted
- Taruya, A., Koyama, K., & Soda, J. 1998, astro-ph/9807005, *ApJ*, accepted
- Taruya, A. & Soda, J. 1998, astro-ph/9809204, *ApJ*, submitted
- Tegmark, M. & Peebles, P. J. E. 1998, *ApJ*, 500, L79
- Tóth, G., Hollósi, J. & Szalay, A. S. 1989, *ApJ*, 344, 75
- Verde, L. *et al.* 1999, in preparation
- White, M. 1998, astro-ph/9811227, *MNRAS*, submitted
- Watson, G. N. 1966, *Theory of Bessel Functions*, Cambridge University Press, Cambridge